1971

X-ray and neutron diffraction study of the holmium-iron system

Michael Fred Simmons

X-RAY AND NEUTRON DIFFRACTION STUDY OF THE HOLMIUM-IRON SYSTEM

by

MICHAEL FRED SIMMONS, 1942-

A DISSERTATION

Presented to the Faculty of the Graduate School of the

UNIVERSITY OF MISSOURI-ROLLA

In Partial Fulfillment of the Requirements for the Degree

DOCTOR OF PHILOSOPHY

in

METALLURGICAL ENGINEERING

1971

W. J. James
Advisor

T. O'Keefe

William A. Fraad

Don M. Spaulin

L. E. Strausmann

ABSTRACT

Neutron diffraction and x-ray powder studies have been made of holmium-iron intermetallic compounds. The magnetic moments of Ho and Fe are in good agreement with measured spontaneous magnetization assuming a ferrimagnetic model with the Ho moments antiparallel to the Fe moments. The magnetic moments of the Fe atoms are found to be localized and thus independent of the rare earth content in the alloys. In contrast to $HoCo_3$, (00ℓ) type magnetic peaks in the neutron diffraction patterns are still prevalent at room temperature and gradually decrease as the Curie temperature is approached. This fact indicates that the easy direction of magnetization remains in the basal plane.

The easy direction of magnetization at room temperature is found to be parallel with the cube edge in $HoFe_2$ and to lie in the basal plane in $HoFe_3$ and Ho_2Fe_{17}. The easy direction is parallel to the a-axis in Ho_2Fe_{17}. It is parallel to the b-direction, i.e. 30° from an a-axis, in the $HoFe_3$ hexagonal cell.

ACKNOWLEDGEMENTS

The author is extremely grateful to Dr. William J. James, Professor of Chemistry and Director of the Graduate Center for Materials Research, for his perpetual optimism, willing discussions, and enthusiastic interest throughout the course of this investigation. He also wishes to express his gratitude to Dr. Thomas J. O'Keefe, Associate Professor of Metallurgical Engineering and Senior Investigator at the Graduate Center for Materials Research, and to Dr. Remy Lemaire, Visiting Professor of Metallurgical Engineering, for their interest and assistance.

Professor Lewis Muhlestein and Mr. Richard Coy of the Physics Department of the University of Missouri-Columbia, Dr. W. C. Koehler of the Oak Ridge National Laboratory, and Drs. Jean Michel Moreau and Christain Michel, Postdoctoral Fellows at the University of Missouri-Rolla, receive special thanks for their instruction and assistance in carrying out the experimental neutron diffraction scans.

The author would also like to thank Dr. Ken Mayhan of the Graduate Center for Materials Research, University of Missouri-Rolla, for preparation of the polyol material used in the x-ray easy direction of magnetization studies and Mr. Robert Crosby and Mr. Harold Huskey for the use of the arc melting facilities of the U.S. Bureau of Mines, Rolla, Missouri.

The financial aid received from the University of Missouri-Rolla and a grant from the Air Force Materials

Laboratory, Dayton, Ohio, is sincerely appreciated.

A particular note of appreciation is extended to the author's wife, Donna, for her support and patience during these graduate studies.

TABLE OF CONTENTS

TABLE OF CONTENTS (continued)

LIST OF TABLES

LIST OF FIGURES

LIST OF FIGURES (continued)

I. INTRODUCTION

While many of the rare earth elements have high atomic magnetic moments, they also have very low Curie (magnetic ordering) temperatures. The development of permanent magnet materials has been to alloy these elements with cobalt and iron having the highest Curie temperatures known. Cobalt, in addition to possessing a moderate magnetic moment, has strong magnetocrystalline anisotropy, a property directly related to high Curie temperatures. Iron has a larger magnetic moment and a somewhat smaller anisotropy than cobalt.

Numerous investigations have been made of the magnetic properties of rare earth-cobalt and rare earth-nickel compounds; however, the need to better understand the alloying behavior of all transition metals requires additional studies using iron. Increased emphasis has been placed on the magnetic behavior of binary compounds containing iron since it was discovered that the Curie temperatures of these compounds increase with increasing rare earth content (in contrast to the behavior of the corresponding compounds with cobalt and nickel). Very recent studies show R_2Fe_{17} compounds to have a negative thermal expansion below their magnetic ordering temperature whereas the analogous compounds containing cobalt and nickel behave normally.

The discovery of $SmCo_5$ as one of the best permanent magnet materials thus far developed played a major role in

increasing interest in rare earth-transition metal alloys. Magnets made of this compound have exhibited an energy product, $(BH)_{max}$, as much as three times that of conventional Alnico magnets and an intrinsic coercive force thirty times greater than that of conventional permanent magnets. Although the magnetic properties of this compound and other rare earth-transition metal compounds are quite well known, there is no satisfactory theory relating magnetic properties to composition.

Since the $CaCu_5$ structure present in $SmCo_5$ is the major "building-block" in the RFe_3 and R_2Fe_{17} structures, a magnetic structure study of these compounds would contribute to a better understanding of the behavior of iron in rare earth-transition metal compounds and to explaining the relationship of the magnetic properties to alloy composition.

Considerable interest has been expressed in the literature by both commercial and scientific circles concerning the desirability of alloys with a stabilized $CaCu_5$ structure wherein the high coercive force of cobalt is complimented by the high remanent and saturation magnetization of iron. In as much as this study and prior ones have shown the magnetic behavior of cobalt and iron to be strikingly different with regard to rare earth content, it is probable that ordering will occur, enhancing the magnetocrystalline anisotropy.

II. LITERATURE SURVEY

When preparing alloys of a binary system a knowledge of the phase diagram is of utmost importance. One of the basic tools in these investigations is metallography. It is extremely helpful in identifying phases and determining homogeneity of samples. The transition temperature and whether a compound melts congruently or decomposes peritectically, are quite influential in selecting the cooling rate for the specimen. They may even be so important as to make certain melting methods unfeasible for some applications. A crystal structure investigation is often complementary to a phase diagram study in the determination of the structure of known existing phases. If the binary system under investigation is of magnetic interest, magnetic structure determinations are performed on the intermetallic compounds and perhaps on specific alloy compositions within a two phase region.

A. Crystal Structures

The holmium-iron phase diagram, shown in Fig. 1, has been studied by Roe and O'Keefe[1]. Four intermediate phases were found: $HoFe_2$, $HoFe_3$, Ho_6Fe_{23}, and Ho_2Fe_{17}. The crystal structure of $HoFe_2$ is isomorphous with the cubic $MgCu_2$ Laves phase[2]; $HoFe_3$ has the rhombohedral $PuNi_3$[3] structure; the cubic Ho_6Fe_{23} is of the Th_6Mn_{23}[4] type. Hexagonal Ho_2Fe_{17} is of the Th_2Ni_{17}[5] type; however, recent investigations by Givord et al.[6] on numerous R_2Fe_{17} single crystals have

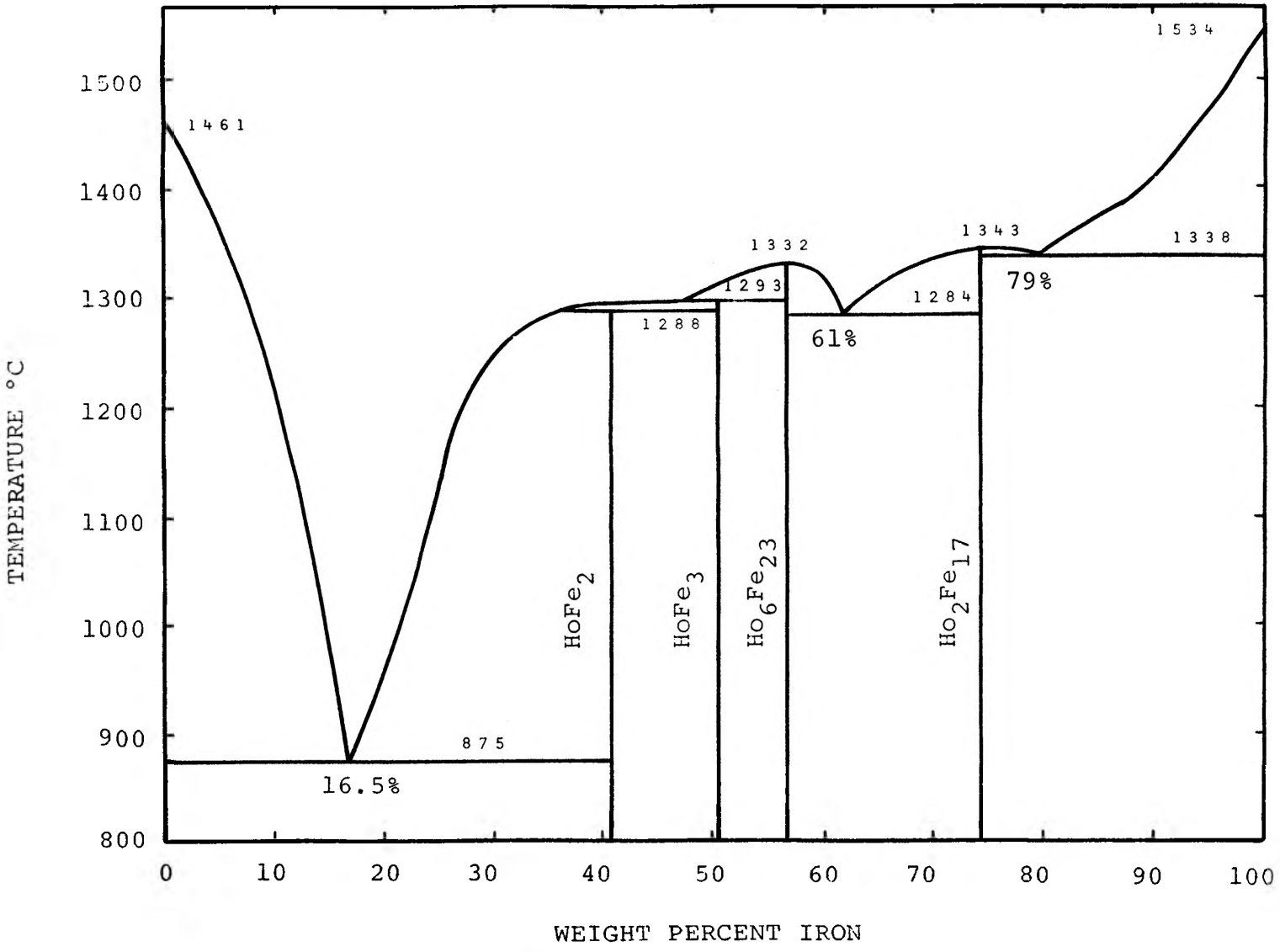

Figure 1. The iron-holmium binary system.

shown that a random substitution of pairs of iron atoms can occur along the c-direction which stabilizes the $CaCu_5$ subcell, resulting in compounds of composition $RFe_{8.5}$ to $RFe_{9.6}$. The lattice parameters determined by x-ray powder methods by O'Keefe, Roe and James[7] are given in Table I.

TABLE I

LATTICE PARAMETERS OF Ho-Fe COMPOUNDS

	$HoFe_2$	$HoFe_3$	Ho_6Fe_{23}	Ho_2Fe_{17}
System	Cubic	Hexagonal	Cubic	Hexagonal
Parameters (A°)	a=7.305	a=5.084 c=24.45	a=12.032	a=8.438 c=8.310
Space Group	Fd3m	$R\bar{3}m$	Fm3m	$P6_3/mmc$

Although an AB_5 compound (see Fig. 2) is not stable in the Ho-Fe system, the crystal structures of the compounds $HoFe_3$ and Ho_2Fe_{17} can be deduced from the AB_5 hexagonal structure[8] by ordered substitutions of atoms.

1. AB_5 Structure

The AB_5 structure is of the $CaCu_5$ type[9] belonging to space group P6/mmm and having the following atom positions:

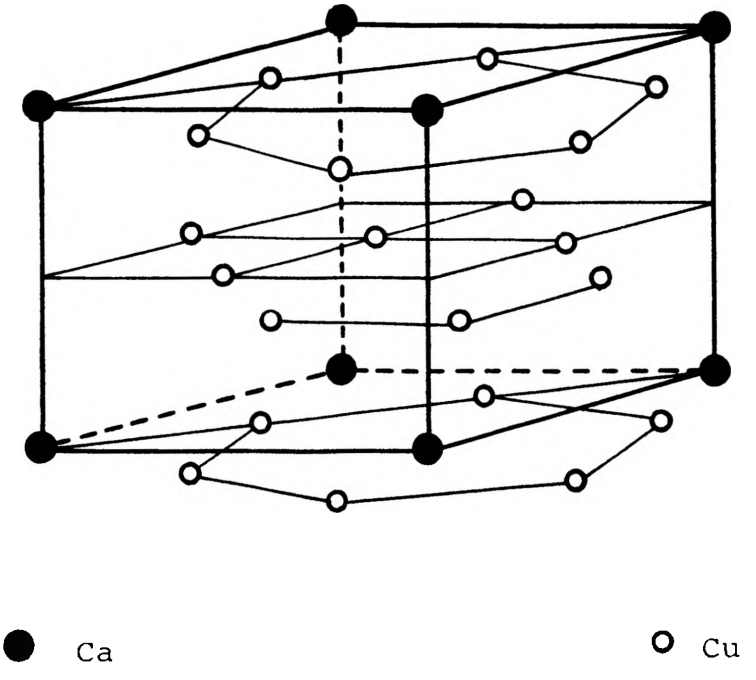

Figure 2. $CaCu_5$ structure

TABLE II

ATOM POSITIONS OF AB_5 STRUCTURE

SPACE GROUP P6/mmm

ATOMS		POSITIONS
1A	1(a)	(0,0,0)
$2B_I$	2(c)	$\pm$(1/3,2/3,0)
$3B_{II}$	3(g)	(1/2,0,1/2);(0,1/2,1/2);(1/2,1/2,1/2)

This structure can be considered as two alternating types of planes. One layer consists of a hexagonal arrangement of B atoms (B_{II}). The other layer can be thought of as being formed by hexagonal arrangements of B atoms (B_I) with an A atom located at the center of the B hexagons (see Fig. 2).

2. Ho_2Fe_{17} Structure

This structure can be derived from the hypothetical "$HoFe_5$" structure by the ordered substitution of a pair of iron atoms for a holmium atom according to the formula:

$$6HoFe_5 - 2Ho + 4Fe = 2Ho_2Fe_{17}.$$

The reason the above formula is expressed in this manner and not reduced to lowest order coefficients is to illustrate more emphatically that crystallographically a unit cell of Ho_2Fe_{17} is composed of two

formula units of the compound. This structure belongs to space group $P6_3/mmc$ having the following atom positions:

TABLE III

ATOM POSITIONS OF Ho_2Fe_{17} STRUCTURE

SPACE GROUP $P6_3/mmc$

ATOMS		POSITIONS
$2Ho_I$	2(b)	$\pm(0,0,1/4)$
$2Ho_{II}$	2(d)	$\pm(1/3,2/3,3/4)$
$6Fe_I$	6(g)	$(1/2,0,0);(0,1/2,0);(1/2,1/2,0);$ $(0,1/2,1/2);(1/2,1/2,1/2)$
$12Fe_{II}$	12(j)	$\pm(x,y,1/4);\pm(\bar{y},x-y,1/4);\pm(y-x,\bar{x},1/4);$ $(\bar{y},\bar{x},1/4);(x,x-y,1/4);(y-x,y,1/4)$ $x=1/3 \quad y=0.975$
$12Fe_{III}$	12(k)	$\pm(x,2x,z);\pm(2\bar{x},\bar{x},z);\pm(x,\bar{x},z);$ $\pm(\bar{x},2\bar{x},1/2+x);(2x,x,1/2+z);$ $\pm(\bar{x},x,1/2+z)$ $x=0.1667 \quad z=0.978$
$4Fe_{IV}$	4(f)	$\pm(1/3,2/3,z);\pm(2/3,1/3,1/2+z)$ $z=0.103$

As can be seen in Fig. 3, the Ho_2Fe_{17} unit cell is composed of six AB_5 type cells. Fig. 4 represents the

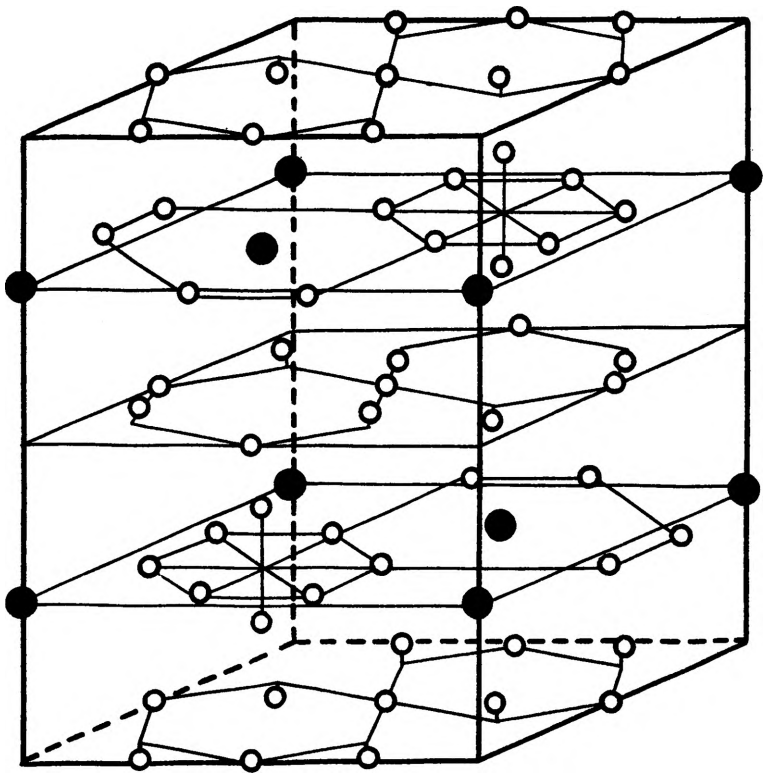

Figure 3. Ho_2Fe_{17} structure.

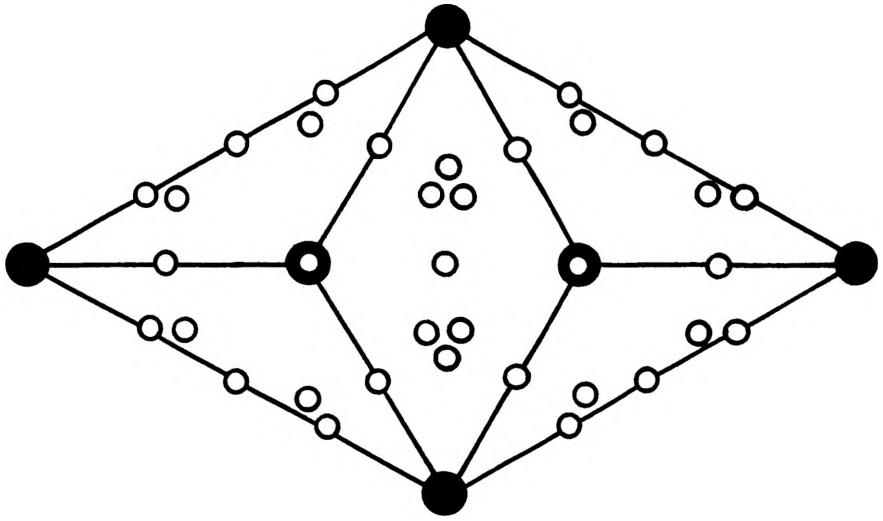

Figure 4. Projection of the Ho_2Fe_{17} cell on basal plane.

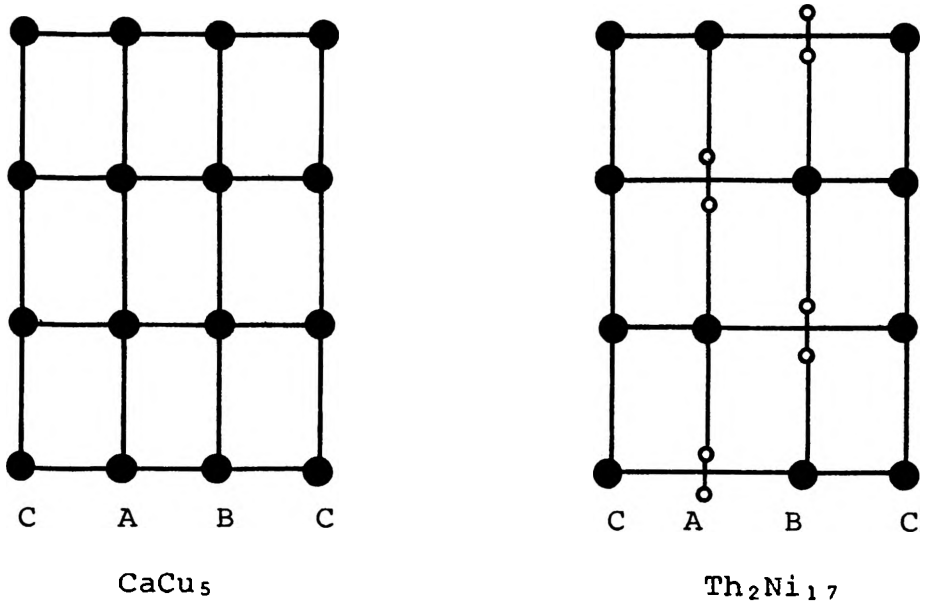

$CaCu_5$ Th_2Ni_{17}

Figure 5. AB AB type substitutional ordering in the Th_2Ni_{17}-type structure.

basal plane projection of the Ho_2Fe_{17} cell and Fig. 5 distinguishes three separate rows of atoms parallel to the c-axis. When the pairs of iron atoms are substituted in rows A and B as shown, the hexagonal Th_2Ni_{17} type structure is obtained.

3. $HoFe_3$ Structure

The $HoFe_3$ structure can be obtained by ordered substitutions of a holmium atom in every second "$HoFe_5$" cell according to the scheme

$$6HoFe_5 - 3Fe + 3Ho = 9HoFe_3.$$

The smallest periodicity of this structure is a rhombohedral cell. For convenience, a hexagonal unit cell is usually chosen which is composed of nine formula units of the compound as indicated by the above equation (which is not reduced to smallest coefficients to again illustrate that this number of atoms are needed to crystallographically describe the cell). This compound belongs to space group $R\bar{3}m$. When it is indexed in the hexagonal system the additional extinction law of $-h+k+\ell=3n$[10] must be applied to all reflections. This extinction rule causes the multiplicity of h0h, 0kℓ and h0ℓ reflections to be reduced from 12 to 6 while hh0 and hhℓ reflections remain at 6 and 12 respectively as in the hexagonal system. Fig. 6 shows the $HoFe_3$ structure. By comparison with Fig. 2 it is seen that this hexagonal cell contains AB_5 type unit cells with a substitution

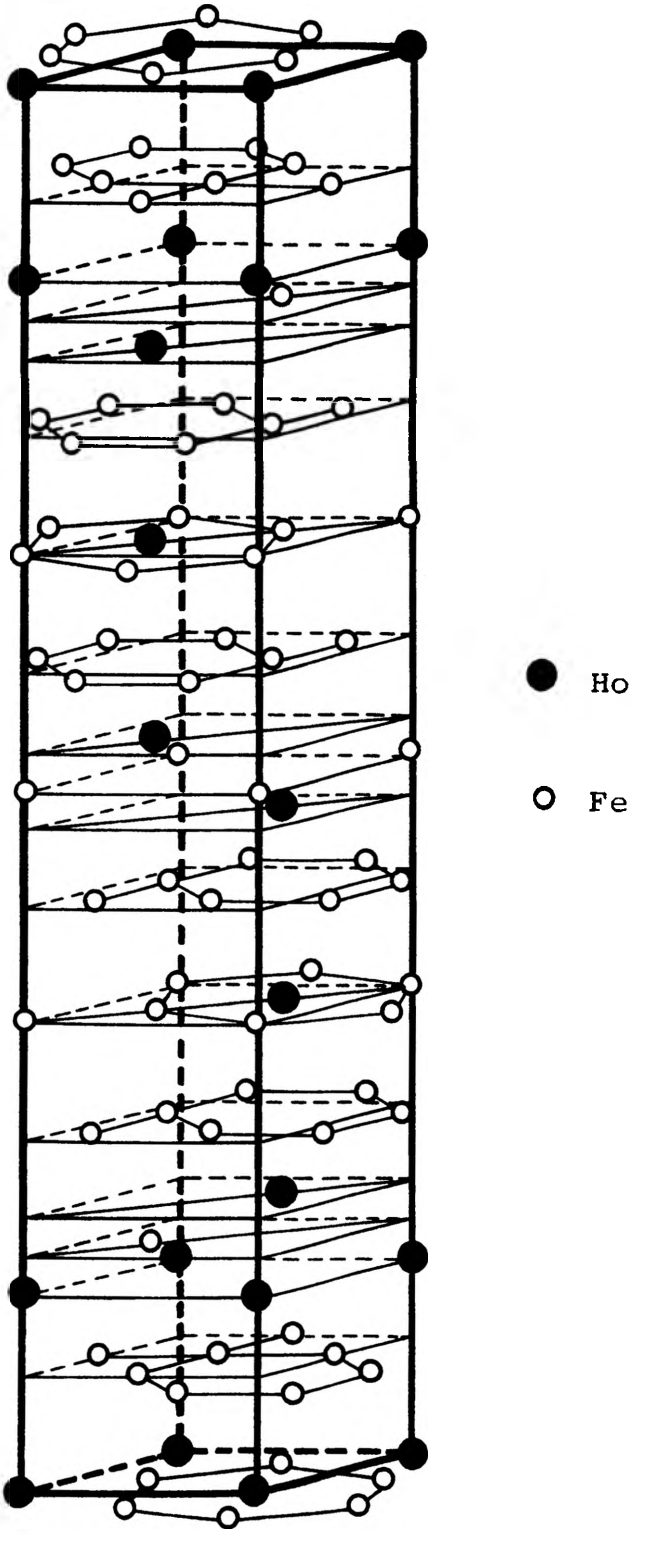

Figure 6. $HoFe_3$ structure.

zone in every second AB_5 unit. The atom positions in $HoFe_3$ are shown in Table IV.

Table IV

ATOM POSITIONS OF $HoFe_3$ STRUCTURE

SPACE GROUP $R\bar{3}m$

ATOMS		POSITIONS
$3Ho_I$	3(a)	(0,0,0)
$6Ho_{II}$	6(c)	$\pm$(0,0,z) z=0.143
$3Fe_I$	3(b)	(0,0,1/2)
$6Fe_{II}$	6(c)	$\pm$(0,0,z) z=1/3
$18Fe_{III}$	18(h)	$\pm(x,\bar{x},z);\pm(x,2x,z);\pm(2\bar{x},\bar{x},z)$ x=1/2 z=0.0789
plus translations		(0,0,0);(2/3,1/3,1/3);(1/3,2/3,2/3)

B. Magnetic Structures

Neutron diffraction methods have been used for magnetic structure determinations of Ho_6Fe_{23}[11] and $HoFe_2$[12]. Both of these compounds have a ferrimagnetic structure below the Curie temperature with the holmium moments antiparallel to the iron moments. The magnetic cell in these compounds is coincidental with the nuclear cell.

A study of the magnetic properties of rare earth-iron RFe_3 compounds by Hoffer and Salmans[13] showed $HoFe_3$ to have

Curie and compensation temperatures of 567 and 405°K respectively and an absolute saturation moment of $4.4\mu_B$ per formula unit. The magnetization curve for $HoFe_3$ in a field of 45 KOe. is shown in Fig. 7.

Neutron diffraction studies of $HoCo_3$ by Schweizer[14] show that the easy direction of magnetization changed from the basal plane at 4.2°K to a direction parallel to the c-axis at room temperature. Fig. 8 shows the neutron diffraction patterns of $HoCo_3$. It is interesting that the (00ℓ) magnetic peaks disappear as the temperature is increased from liquid helium to room temperature, indicating the change in the easy direction of magnetization.

C. X-Ray Diffraction - Easy Direction of Magnetization

A very convenient method of determining the easy direction of magnetization was developed by Lemaire[15]. His method consists of placing very finely ground powder in a magnetic field so that the powder particles form needles. The needles are then bonded with glue and x-ray patterns taken. The resulting diffraction patterns show spots of increased intensity indicating a very strong texture or preferred orientation. The easy direction of magnetization can be deduced from the location of the spots analogous to determining crystal orientation by means of the rotating-crystal method.

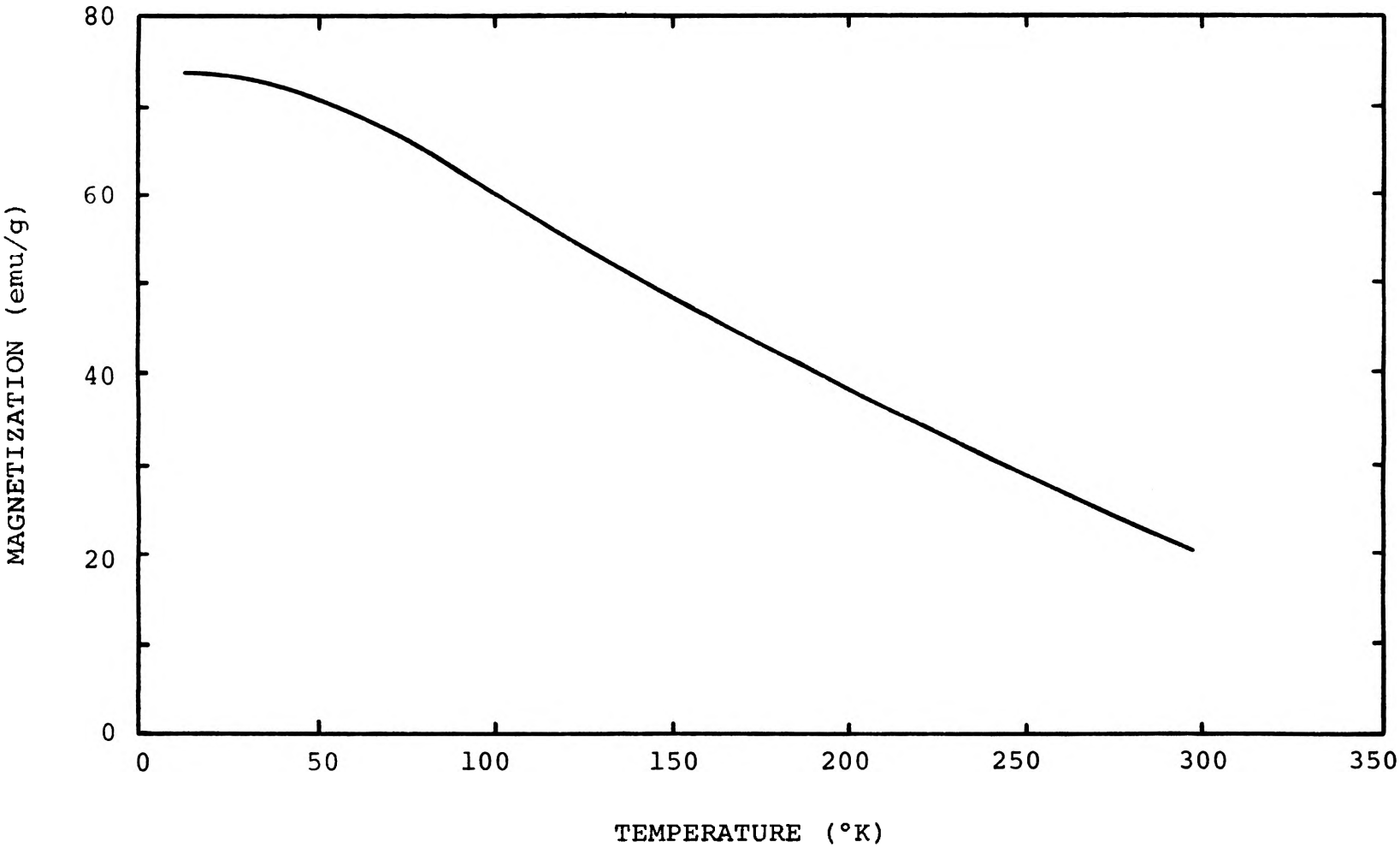

Figure 7. Magnetization versus temperature curve for $HoFe_3$ in 45KOe. magnetic field.

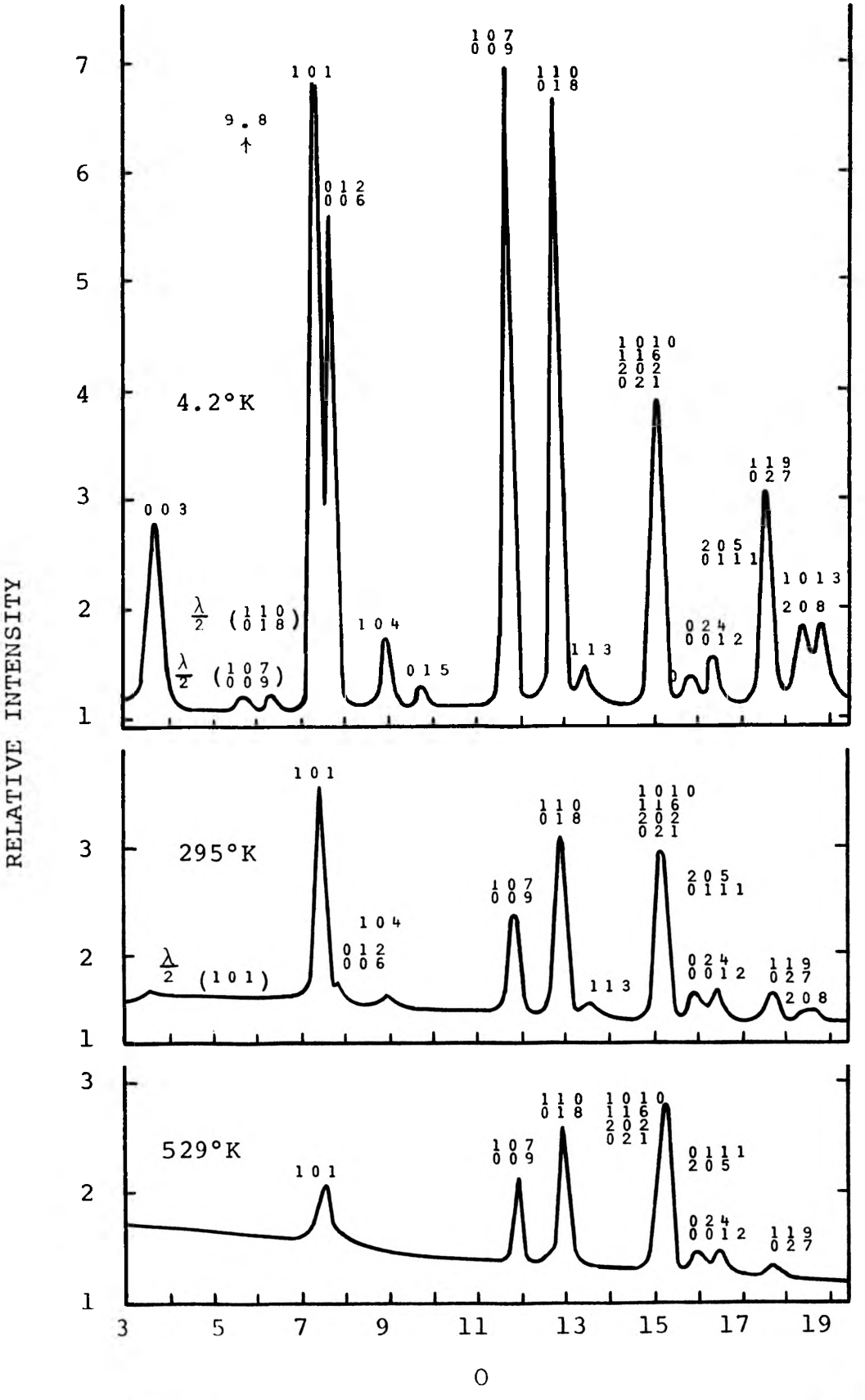

Figure 8 Neutron diffraction patterns of $HoCo_3$

III. EXPERIMENTAL PROCEDURE

A. Materials

1. Holmium. The holmium was obtained from Lunex Company, Pleasant Valley, Iowa. It was in 1/4 inch diameter bar form and of 99.9+% purity.

2. Iron. The iron used was supplied by Bethlehem Steel Corporation, Bethlehem, Pennsylvania and was of 99.9+% purity.

B. Melting Procedures

Both arc melting and induction melting methods were used in alloy preparation. The $HoFe_3$ sample used in this investigation was prepared by arc melting although samples have been induction melted which showed no second-phase lines upon x-ray examination. The $HoFe_2$ and Ho_2Fe_{17} samples were obtained from Professor William J. James and had been prepared by induction melting by Dr. Gerald Roe during previous investigations[16] of the holmium-iron system. The initial samples used for the exploratory studies mentioned in the Future Studies section of this thesis were prepared by induction melting.

Arc melting was used primarily to take advantage of the rapid cooling rate obtained from the water-cooled, copper hearth. This is important in preparing the pertictically formed $HoFe_3$ in order to reduce the amount of second phase. The fact that no alumina crucible is required decreases

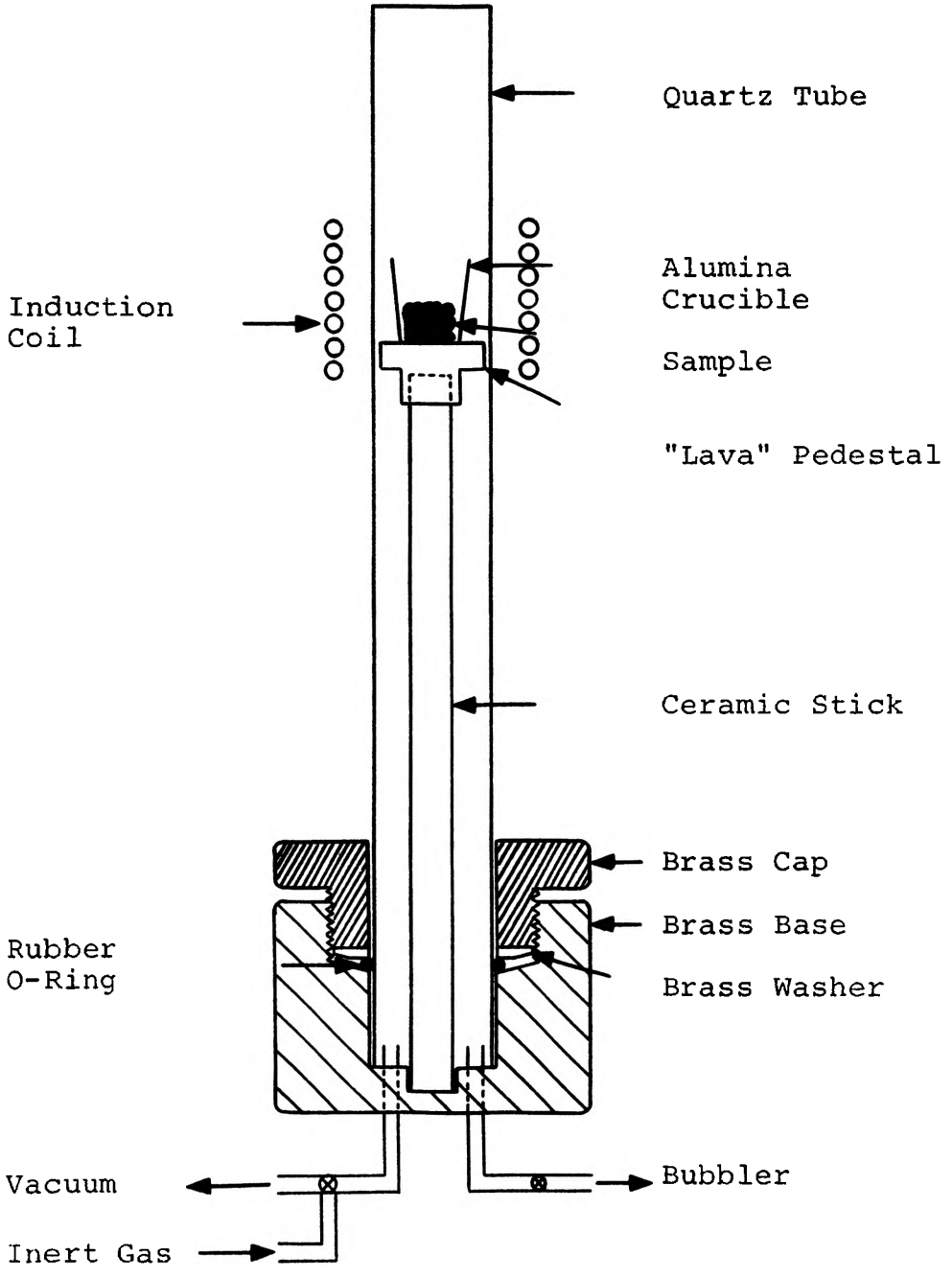

Figure 9. Cross-sectional view of induction furnace.

the possibility of contamination. All arc melting was done at the U.S. Bureau of Mines, Rolla, Missouri, using a nonconsumable tungsten electrode.

Induction melting was carried out in a small inert gas chamber consisting of a quartz tube with one end sealed. The open end of this tube was sealed by means of an O-ring to a brass base to which a pedestal of fired "lava" was mounted. The pedestal stands within the quartz tube. A detailed drawing of this induction melting chamber is shown in Fig. 9.

1. Arc Melting

The following procedure was used for all arc melted samples:

a. Place the samples on a copper hearth in separate molds and evacuate the system.

b. Flush the system twice with high purity helium.

c. Reevacuate the system to 4.5×10^{-5} torr.

d. Bleed in helium to 12 inches of Hg pressure.

e. Turn the power on to approximately 150 amps.

f. Melt the titanium getter button in the center of the hearth.

g. Melt the sample, then slowly cut back the power to reduce the cooling rate.

h. Remelt the titanium getter after melting each sample if more than one sample is being prepared.

i. Turn over the getter and the samples using the tip of the wand and remelt as in step g and h above.

2. Induction Melting

The following procedure was used for all induction melted samples:

a. Place the samples in the alumina crucible and center it on the pedestal in the quartz tube.

b. Tighten the O-ring seal on the bottom of the tube.

c. Evacuate and flush the system with high purity argon four times by means of the 3-way valve.

d. Set the argon regulator so that a very slow flow is going through the system.

e. Start up the 5kw. generator and turn up the power very slowly until the sample melts.

f. Allow the sample to remain in the molten state for approximately five minutes to assure homogenization.

g. Reduce the power rapidly for a peritectic compound or slowly if a congruent compound is being prepared.

h. Allow the system to cool to room temperature.

C. X-Ray Diffraction

Powder x-ray diffraction techniques were employed to

identify the phases present in "as-cast" alloys. Another important use of x-ray diffraction in this investigation was that of determining the easy direction of magnetization of these intermetallic compounds by means of a preferred orientation effect.

1. Phase Identification

Particles chosen at random from a broken, as-cast sample were ground by means of a mortar and pestle in a glove bag under an argon atmosphere. The powder was then screened through a 325 mesh (44 micron) screen. The powder was then mounted on a quartz fiber coated with vaseline or placed inside a 0.3 mm. diameter glass capillary. The mounted powder sample was then aligned and centered in a Straumanis camera using asymmetrical film loading. Iron, cobalt, and chromium radiation were used at various times both with and without filters.

2. Easy Direction of Magnetization Determinations

Some of the same powder used for the normal x-ray powder pattern was suspended in a few drops of a long chain polyol to which had been added a curing agent of an isocynate. This mixture was prepared in a small nonmagnetic container, e.g., aluminum foil dish. The dish containing the mixture was placed between the poles of an electromagnet and the magnetic field slowly increased to the point where small needles were

formed on the side of the dish. When difficulty was encountered in forming needles, they could be made by holding a small nonmagnetic stick near the magnet pole with some of the mixture on the end. The polyol and curing agent usually hardened within an hour and formed a thin transparent film around the needles, thus holding the powder particles in their preferred orientation. After hardening, the magnetic field was shut off and the needles aligned and x-rayed as for standard powder samples.

If the powder is strongly preferentially oriented, the pattern will conform to that from a disordered, single crystal. Thus we observe elongated "spots" as opposed to "lines". Analysis of these spots was made as in the rotating-crystal method[17,18]. It must be pointed out that particles of elongated shape or needle-like shape can not be used for this type of experiment since such particles would tend to align along the long axis irrespective of their crystallographic easy direction of magnetization[19].

D. Neutron Diffraction

1. Experimental Technique

Neutron diffraction of a Ho_2Fe_{17} sample was carried out at Oak Ridge National Laboratory, Oak Ridge, Tennessee, by Drs. Jean Michel Moreau and Christain Michel[20]. The analysis of these data was

performed by the author. The experiment and the analysis of the neutron diffraction data of $HoFe_3$ was done at the University of Missouri, Columbia, Missouri, by the author. X-ray powder patterns of both samples had previously indicated single phase material. High and low temperature neutron diffraction patterns were run on both samples. Low temperature runs ($T<<T_c$) at liquid nitrogen temperature provided the data necessary to determine the magnitude of the atomic magnetic moments and the magnetic structure of the intermetallic compounds. High temperature scans above the appropriate Curie temperatures gave data determining the nuclear structure and corresponding intensities. The nuclear intensities must be evaluated before an accurate magnetic structure determination can be made.

The alloys were crushed and placed in an aluminum cylindrical cell. For low temperature runs, the aluminum sample cell was placed in a cryostat which was subsequently cooled to liquid nitrogen temperature. The high temperature runs were made in a resistance furnace which could be controlled to $\pm 1°C$. The furnace runs were made at approximately 25°C above the Curie temperature of the sample so that short range magnetic order would be absent.

Before diffraction data were collected, proper alignment was verified by taking a polaroid photograph of the sample in the neutron beam. Scans were made

of the samples from 5-40° in 2θ at 0.1° increments. The diffracted beam count was done in three separate periods, each having a monitor count of 10,000. The diffracted beam count in each of the three periods was then summed to give the total count per angle. This was done so that if a questionable count were obtained in a given period, it could be discarded and the remaining two periods averaged to give a replacement count. If more than one period of the three were questionable, that angle was rerun.

Room temperature runs of the $HoFe_3$ sample were made in both the cryostat and furnace for comparison. It was found that the pattern reproduced within the accuracy of the data so that no correction had to be made for absorption effects due to the cryostat or furnace. Scans were made however of the empty sample cell in the furnace and cryostat so that their individual contributions could be subtracted from the sample diffraction patterns. No attempt was made to determine absolute intensity values.

2. Nuclear and Magnetic Calculations

The relative intensity of a neutron powder diffraction peak is given by Eq. (1).

$$I_n = \frac{m \mid F_n \mid^2 \exp[-2B(\sin^2\theta/\lambda^2)]}{\sin\theta \sin 2\theta} \qquad (1)$$

where:

I_n = relative nuclear intensity of neutron powder diffraction peak.

m = multiplicity of the reflection.

F_n = nuclear structure factor.

B = temperature correction factor.

θ = Bragg angle of diffraction.

λ = neutron wavelength.

The nuclear structure factor is given by the following equation.

$$F_n = \Sigma b \exp 2\pi i(hx/a_o + ky/b_o + lz/c_o) \quad (2)$$

The nuclear scattering amplitude, b, is equal to 0.85×10^{-12} and 0.96×10^{-12} cm.[21] for holmium and iron respectively.

For low temperature data where the peak intensities are due both to nuclear and to magnetic coherent scattering, F_n in Eq. (1) is replaced by an effective structure factor F.

$$F^2 = F_n^2 + q^2 F_m^2 \quad (3)$$

where:

F = effective structure factor when both nuclear and magnetic contributions are present.

F_n = nuclear structure factor.

$\vec{q}$ = magnetic interaction vector.

F_m = magnetic structure factor.

Substitution of F^2 (3) into (1) for F_n^2 defines I_n and

I_m. The magnetic interaction vector $\vec{q}$ is defined by

$$\vec{q} = \vec{\varepsilon}(\vec{\varepsilon}\cdot\vec{K}) - \vec{K} \qquad (4)$$

where $\vec{K}$ is a unit vector in the direction of the atomic magnetic moment and $\vec{\varepsilon}$, the scattering vector, is a unit vector normal to the scattering plane. A brief discussion of the determination of q^2 is given in Appendix A. An excellent article by Shirane[22] illustrates more thoroughly the calculation of q^2 values for various crystal symmetries in which the magnetic structure is colinear.

The magnetic structure factor, F_m, is given by the following equation (which is very similar to that defining the nuclear structure factor).

$$F_m = \Sigma p \exp 2\pi i(hx/a_o + ky/b_o + lz/c_o) \qquad (5)$$

The magnetic scattering amplitude, p, is calculated using the following equation.

$$p = (e^2\gamma/2mc^2)\vec{\mu}f \qquad (6)$$

where:

p = magnetic scattering amplitude.

e = electron charge

γ = magnetic moment of neutron in nuclear magnetons.

m = neutron mass.

c = velocity of light.

$\vec{\mu}$ = atomic magnetic moment.

f = form factor for magnetic scattering.

The magnetic form factors for holmium and iron are given in Appendix B. Calculations of I_n and I_m, the nuclear and magnetic intensities, were performed using the least-squares refinement program UICCLS1 obtained from Dr. Kahn of the University of Illinois Chicago Campus.

IV. EXPERIMENTAL RESULTS AND DISCUSSION

A. Magnetic Structures

High and low temperature neutron diffraction scans from 5-40° in 2θ were conducted on powder samples of Ho_2Fe_{17}[20] and $HoFe_3$. Both samples had previously exhibited single phase x-ray powder patterns.

The neutron diffraction patterns of Ho_2Fe_{17} and $HoFe_3$ are shown in Figs. 10 and 11 respectively. As these figures illustrate, a considerable difference in intensities is observed between the high and low temperature patterns. The high temperature run, which was at least 25°C above the Curie temperature of the sample, gave the data necessary to determine the nuclear structure of the compound. The increased intensity at liquid nitrogen temperature is due primarily to increased magnetic order which occurs with decreasing temperature.

The calculated and observed intensities for Ho_2Fe_{17} at 633 and 77°K respectively are shown in Tables V and VI. The reliability factor, R, is defined as

$$R = \frac{\Sigma |I_{OBS} - I_{CALC}|}{\Sigma I_{OBS}}$$

Values of R = .008 for I_n and R=.04 for I_m were obtained after refinement.

Normally a scale factor is established during the nuclear refinement which makes the calculated intensities of the same order of magnitude as those observed. This

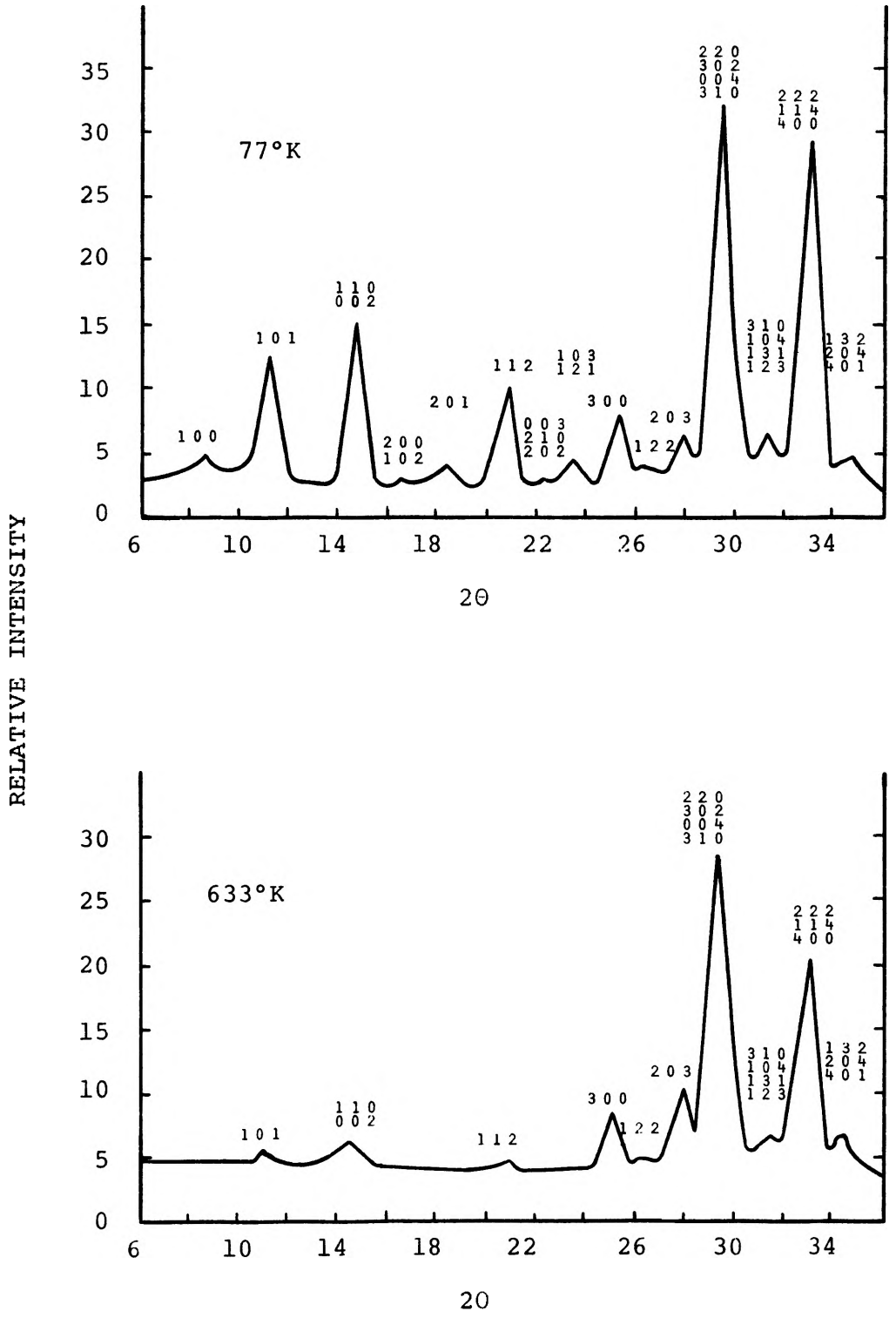

Figure 10. Neutron diffraction patterns of Ho_2Fe_{17}.

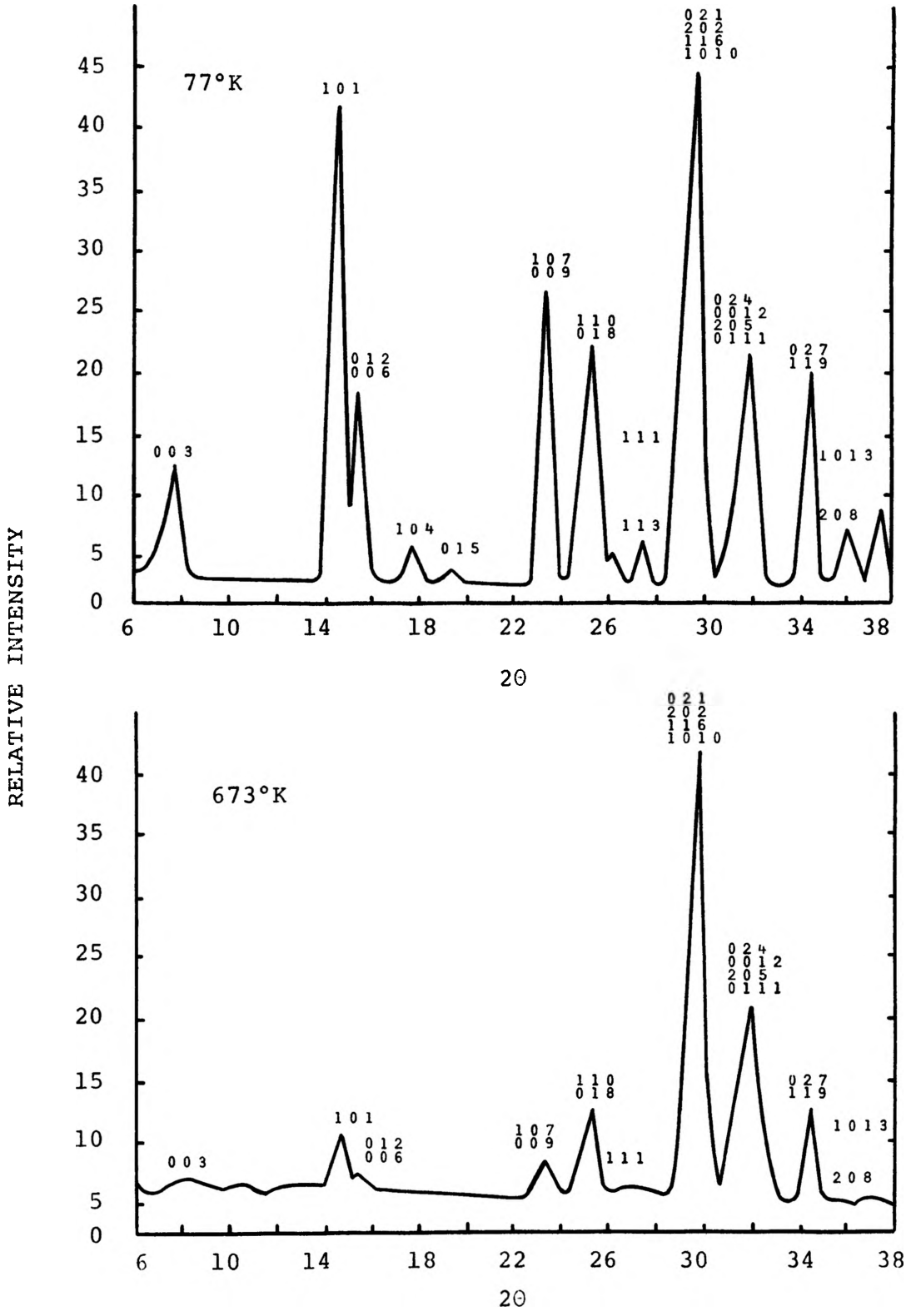

Figure 11. Neutron diffraction patterns of $HoFe_3$.

TABLE V

CALCULATED AND OBSERVED INTENSITIES

FOR Ho_2Fe_{17} AT 633°K

hkℓ	$I_{OBS.}$	$I_{CALC.}$	hkℓ	$I_{OBS.}$	$I_{CALC.}$
001	0.0	0.0	122	14.94	15.12
100	12.19	12.24	203	443.89	446.14
101	10.48	4.71	220	1585.39	1585.55
110	48.77	79.66	302	1518.42	1519.87
002	24.43	39.89	004	3215.67	3215.09
111	0.0	0.0	221	0.0	0.0
200	0.0	0.1	310	21.32	21.43
102	0.0	3.90	104	11.42	11.63
201	0.0	0.35	131	18.91	19.25
112	29.03	26.72	123	63.29	63.81
003	0.0	0.0	222	1631.48	1629.99
210	0.47	1.89	114	467.10	468.13
202	19.14	19.28	303	0.0	0.0
121	1.89	1.84	400	44.04	43.95
103	23.22	23.49	132	0.23	0.26
300	662.21	661.66	204	75.08	76.22
301	0.0	0.0	401	137.89	139.09
113	0.0	0.0			

TABLE VI

CALCULATED AND OBSERVED INTENSITIES

FOR Ho_2Fe_{17} AT 77°K

hkℓ	$I_{OBS.}$	$I_{CALC.}$	hkℓ	$I_{OBS.}$	$I_{CALC.}$
001	0.0	0.0	122	6.55	5.13
100	34.94	29.76	203	7.76	3.24
101	124.02	109.13	220	19.11	16.09
110	313.50	318.18	302	26.53	24.62
002	581.14	585.76	004	7.29	0.46
111	0.0	0.0	221	0.0	0.0
200	13.85	10.86	310	16.45	18.50
102	20.48	16.11	104	8.38	7.59
201	49.05	47.35	131	47.87	53.00
112	276.40	261.70	123	17.09	14.77
003	0.0	0.0	222	475.79	462.41
210	13.38	14.21	114	483.49	499.61
202	6.16	6.07	303	0.0	0.0
121	39.32	40.66	400	18.28	19.56
103	42.10	40.06	132	9.44	9.08
300	58.90	48.13	204	2.66	1.03
301	0.0	0.0	401	58.15	67.69
113	0.0	0.0			

same factor is retained for the magnetic structure determination. However, in the case of Ho_2Fe_{17} a better fit of the low temperature data was obtained when the scale factor was changed from 2.2268 for nuclear intensities to 1.9096 for the magnetic intensities. It is not known what occurred between these runs to necessitate such a change. One possible cause was that the monitor count for the incident neutrons may have been changed between runs, allowing a different neutron flux to impinge upon the sample than had previously been used. The same might have resulted if a greater volume of sample was used in the furnace than in the cryostat.

The atomic magnetic moments obtained from refinement of intensity data for Ho_2Fe_{17} are shown in Table VII.

TABLE VII

ATOMIC MAGNETIC MOMENTS OF

Ho_2Fe_{17} AT 77°K

Atom	Ho_I	Ho_{II}	Fe_I	Fe_{II}	Fe_{III}	Fe_{IV}
Magnetic Moment μ_B	9.37	10.07	2.08	2.07	1.92	2.37

These values result in an average moment for holmium of $9.72\mu_B$ and an average moment for iron of $2.11\mu_B$.

The magnetic structure of Ho_2Fe_{17} is ferrimagnetic

TABLE VIII

CALCULATED AND OBSERVED INTENSITIES

For $HoFe_3$ AT 77°K

hkℓ	$I_{OBS.}$	$I_{CALC.}$	hkℓ	$I_{OBS.}$	$I_{CALC.}$
003	24.10	29.32	021	27.39	27.44
101	104.20	105.56	202	0.30	0.00
012	5.80	5.88	116	27.18	26.10
006	181.49	183.63	10 10	10.02	9.96
104	16.12	15.70	024	3.50	2.52
015	6.42	6.58	00 12	13.49	5.54
107	150.10	149.70	205	23.41	20.06
009	7.81	7.76	01 11	3.25	1.57
110	79.56	77.91	027	145.65	145.65
018	62.21	61.39	119	1.47	1.23
113	8.42	8.37	208	64.17	64.37

TABLE IX

CALCULATED AND OBSERVED INTENSITIES

FOR $HoFe_3$ AT 297°K

hkℓ	$I_{OBS.}$	$I_{CALC.}$	hkℓ	$I_{OBS.}$	$I_{CALC.}$
003	14.34	13.06	021	7.09	5.81
101	45.47	44.46	202	0.66	0.25
012	2.49	2.48	116	7.72	5.64
006	87.75	85.56	10 10	3.82	3.35
104	8.07	7.05	024	0.75	0.40
107	53.31	48.89	00 12	9.30	7.92
009	3.74	3.43	205	12.18	11.68
110	25.98	27.42	01 11	0.56	0.12
018	16.72	17.98	027	60.00	62.67
113	3.17	3.17	119	0.00	0.23
			208	28.96	26.57

TABLE X

CALCULATED AND OBSERVED INTENSITIES

FOR $HoFe_3$ AT 673°K

hkℓ	$I_{OBS.}$	$I_{CALC.}$	hkℓ	$I_{OBS.}$	$I_{CALC.}$
101	14.94	13.33	10 10	5.38	5.50
012	1.79	1.60	024	37.23	36.90
006	3.88	3.46	00 12	333.14	330.25
107	27.40	25.54	205	151.06	149.78
009	0.0	0.0	01 11	61.85	61.32
110	54.73	52.67	027	99.08	100.29
018	44.31	42.65	119	14.89	15.08
113	0.15	0.14			
021	103.93	106.41			
202	53.62	54.91			
116	184.32	188.74			

with iron moments antiparallel to the holmium moments. All magnetic moments are found to lie in the basal plane of the hexagonal structure. This is shown by the best fit of q^2 values, and also by preferred orientation x-ray studies to be discussed in the next section.

Calculated and observed intensities at 77°K, 297°K, and 673°K for $HoFe_3$ are shown in Tables VIII, IX, and X respectively. Reliability factors of R=.019 for I_n, R=.026 for $I_{m,77°K}$, and R=.064 for $I_{m,297°K}$ were obtained. The refined values for the atomic magnetic moments of $HoFe_3$ are shown in Table XI.

TABLE XI

ATOMIC MAGNETIC MOMENTS OF

$HoFe_3$ AT 77°K AND 297°K

°K	Atom	Ho_I	Ho_{II}	Fe_I	Fe_{II}	Fe_{III}
77	Magnetic Moment	8.76	9.01	1.88	1.43	1.61
297	μ_B	5.07	5.42	1.49	1.12	1.52

Average magnetic moments of $8.88\mu_B$ and $5.24\mu_B$ for holmium and $1.64\mu_B$ and $1.38\mu_B$ for iron are found at liquid nitrogen and room temperatures respectively. It will be noticed that $HoFe_3$ is not saturated at 77°K in agreement with the saturation magnetization curve of Hoffer and Salmans[13]

shown in Fig. 7. Saturation occurs at approximately 20°K for an applied field of 45 KOe. according to their magnetization curve.

Although saturation values for the atomic magnetic moments would be desirable, a liquid helium neutron diffraction scan is not necessary. The magnetic structure can be satisfactorily deduced from either the liquid nitrogen or room temperature data.

The magnetic structure of $HoFe_3$ is also found to be ferrimagnetic with the iron moments opposite to those of holmium. The best agreement between observed and calculated intensities is again obtained when q^2 values correspond to the magnetic moments in the basal plane. X-ray studies of $HoFe_3$ provided additional evidence that the moments are actually in the basal plane of the hexagonal cell.

B. X-Ray Study of Easy Direction of Magnetization

The easy directions of magnetization at room temperature of $HoFe_2$, $HoFe_3$, and Ho_2Fe_{17} were determined using the powder x-ray diffraction techniques discussed in a preceding section. Powder patterns of $HoFe_2$, $HoFe_3$, and Ho_2Fe_{17} before and after alignment in a magnetic field of approximately 5KOe. are shown in Figs. 12-14 respectively.

The easy direction of magnetization in $HoFe_2$ is found to be along the cube edge, {100}, in agreement with Mossbauer studies by Bowden[23]. The easy direction of magnetization is found to be in the basal plane for both $HoFe_3$ and Ho_2Fe_{17}.

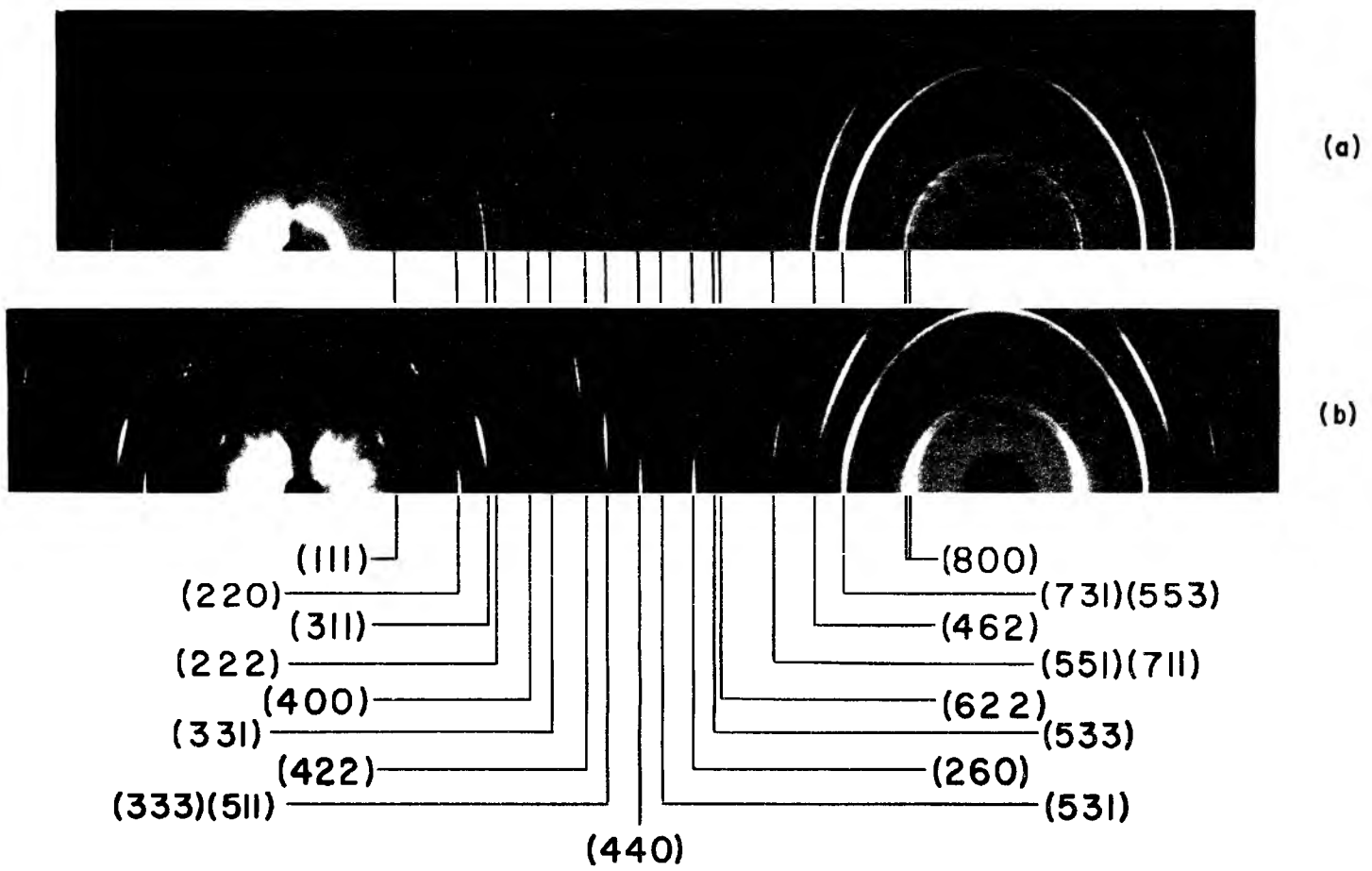

Figure 12. X-ray powder patterns of $HoFe_2$ before (a) and after (b) alignment in magnetic field.

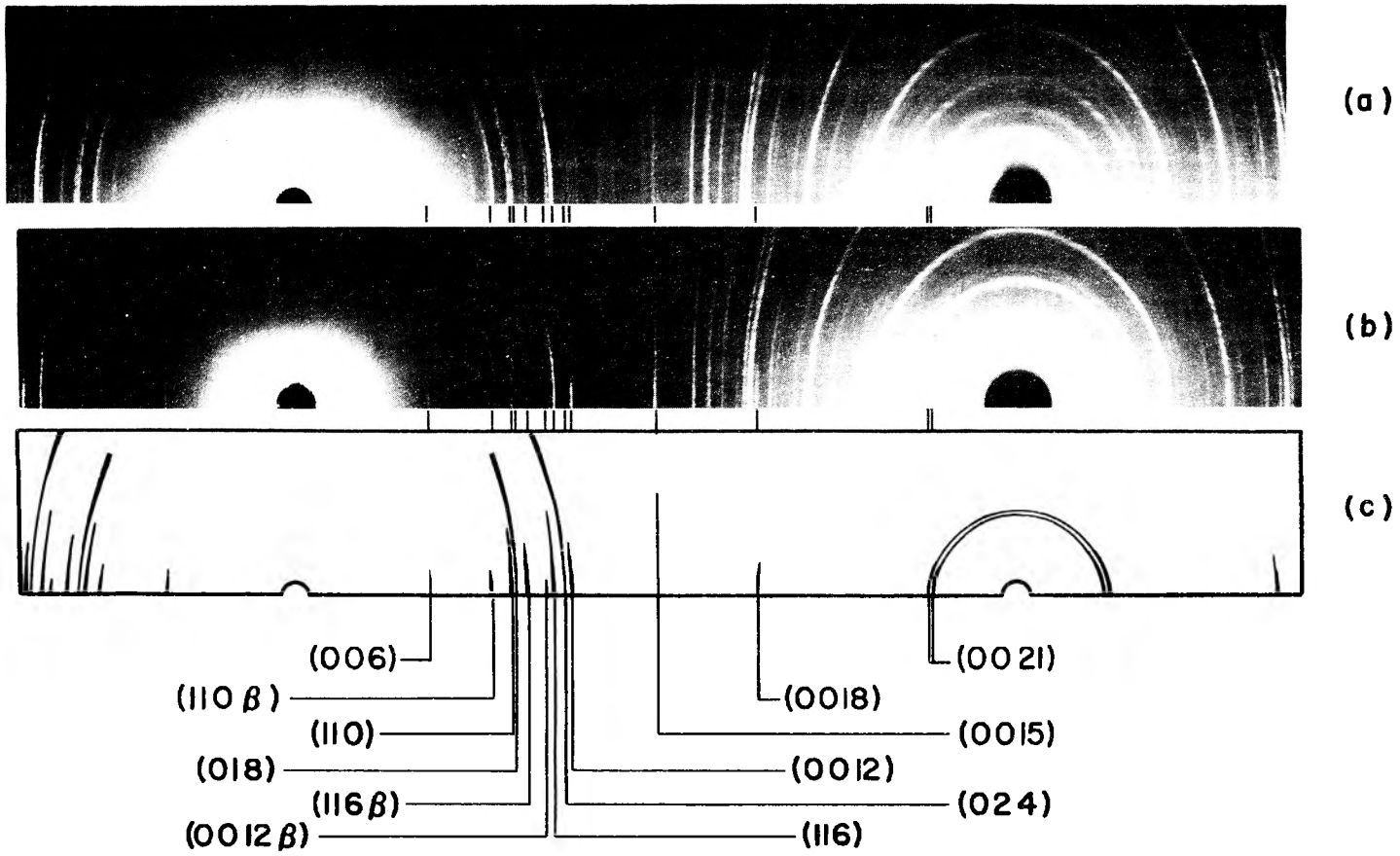

Figure 13. X-ray powder patterns of $HoFe_3$ before (a) and after (b) alignment in magnetic field.

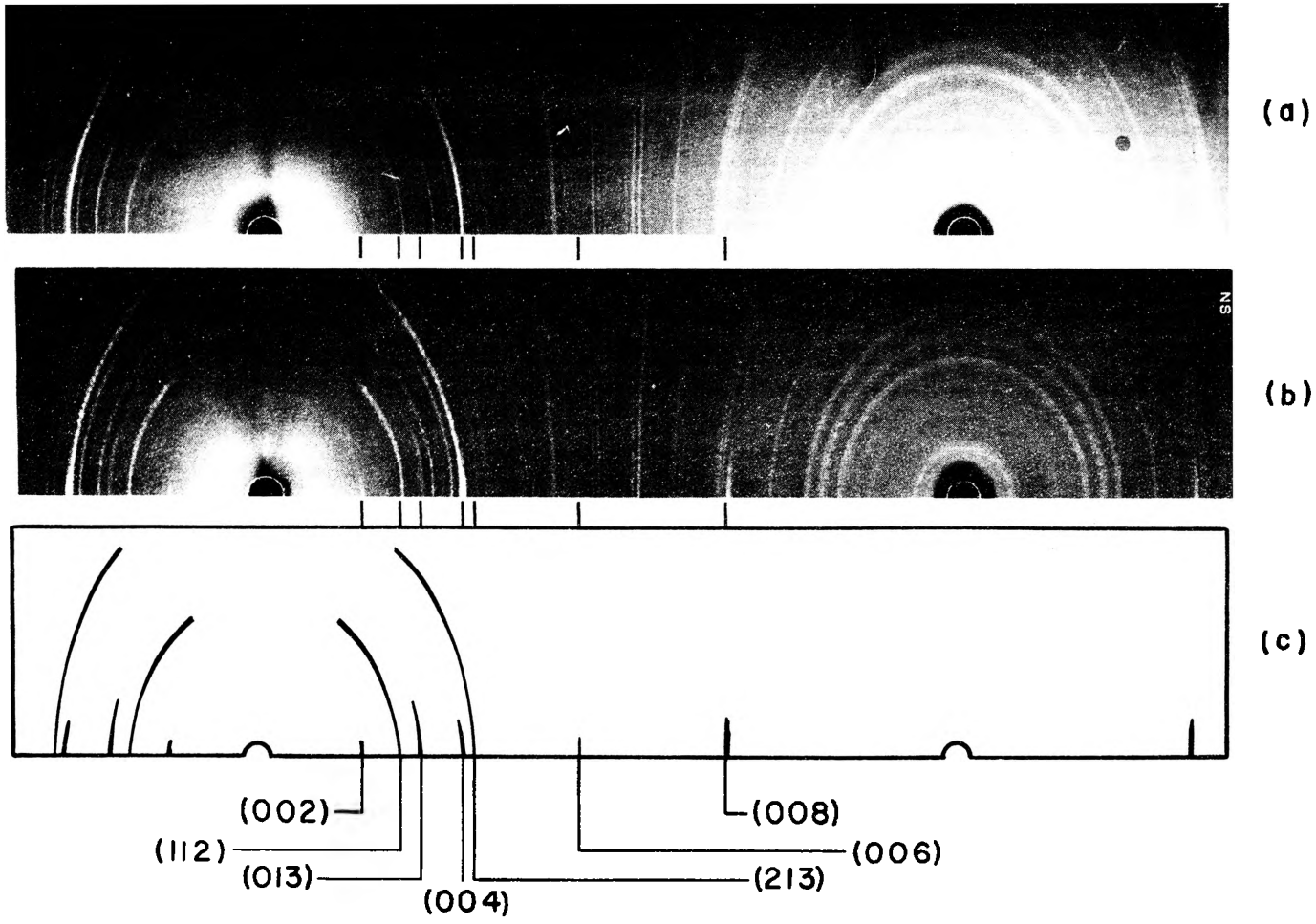

Figure 14. X-ray powder patterns of Ho_2Fe_{17} before (a) and after (b) alignment in magnetic field.

Examination of Fig. 12 for $HoFe_2$ shows that hk0 or h00 reflections are the only ones exhibiting definite "spots". First-level spots are found for hk1 reflections, second-level spots for hk2, and third-level for hk3 reflections. In this f.c.c. structure only all-even or all-odd indices are allowed, thereby eliminating certain orders of the reflections. This pattern of spots corresponds to the easy direction of magnetization being a {100} direction.

Spots are most evident for {00ℓ} reflections in Fig. 13 for $HoFe_3$ indicating that the easy direction of magnetization lies within the basal plane of the hexagonal cell. In order to determine the direction of easy magnetization within the basal plane, additional reflections must be studied. It is found that the observed intensity spots obey the following rules:

h,h,ℓ	0-layer
h,h+1,ℓ	1-layer
h,h+2,ℓ	2-layer

The most evident zero-layer lines are (110), (110β), (116) and (116β). First-layer reflections are seen in the (018) line, where h=0. The zero-layer reflection (008) is not observed since it does not satisfy the rhombohedral extinction rule

$$-h + k + \ell = 3n$$

for allowed reflections[10]. The (024) line is more intense in the second-layer region and is definitely weaker on the first and zero-layers. This is the second-order reflection

of (004) which is not allowed. The (024) line follows the expected rule for second-layer reflections of $(h,h+2,\ell)$. The above extinction effects indicate that the easy direction of magnetization of $HoFe_3$ lies in the b-direction defined as being 30° from a conventional a-axis in the hexagonal cell. The b-direction is illustrated in Fig. 15 where the basal plane of $HoFe_3$ is shown.

At first glance the powder pattern of Ho_2Fe_{17} shown in Fig. 14 appears to be very similar to that of $HoFe_3$. The $\{00\ell\}$ reflections show zero-level spots, again indicating that the easy direction of magnetization lies in the hexagonal basal plane. However, in Ho_2Fe_{17} the following rules appear to be obeyed by the observed spots:

$0,k,\ell$	0-layer
$1,k,\ell$	1-layer
$2,k,\ell$	2-layer

which are indicative of alignment along the hexagonal a-axis.

Consider the (112) line and compare it with the magnetically unaligned pattern. It is definitely more intense in the first-layer region. If this line is considered a $(1k\ell)$ type, and since it shows a strong zero-layer intensity, the easy direction of magnetization must be in the b-direction, as in $HoFe_3$. This is not the case. Additional evidence that the direction lies along the a-axis is found in the (013) zero-layer line and in the (213) second-layer line. Although there is not as much evidence in the case of Ho_2Fe_{17} as for $HoFe_2$ and $HoFe_3$, it appears

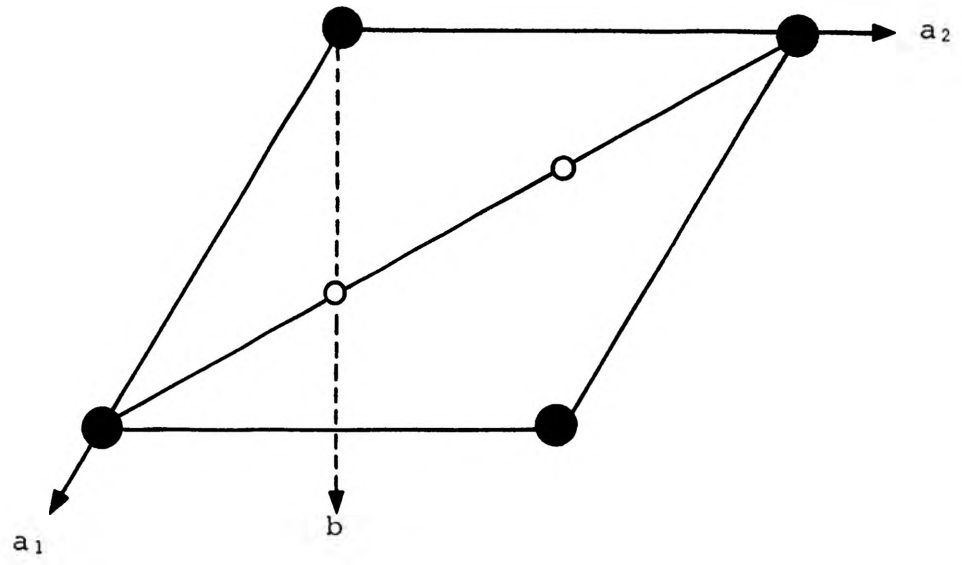

Figure 15. $HoFe_3$ basal plane with b-direction indicated.

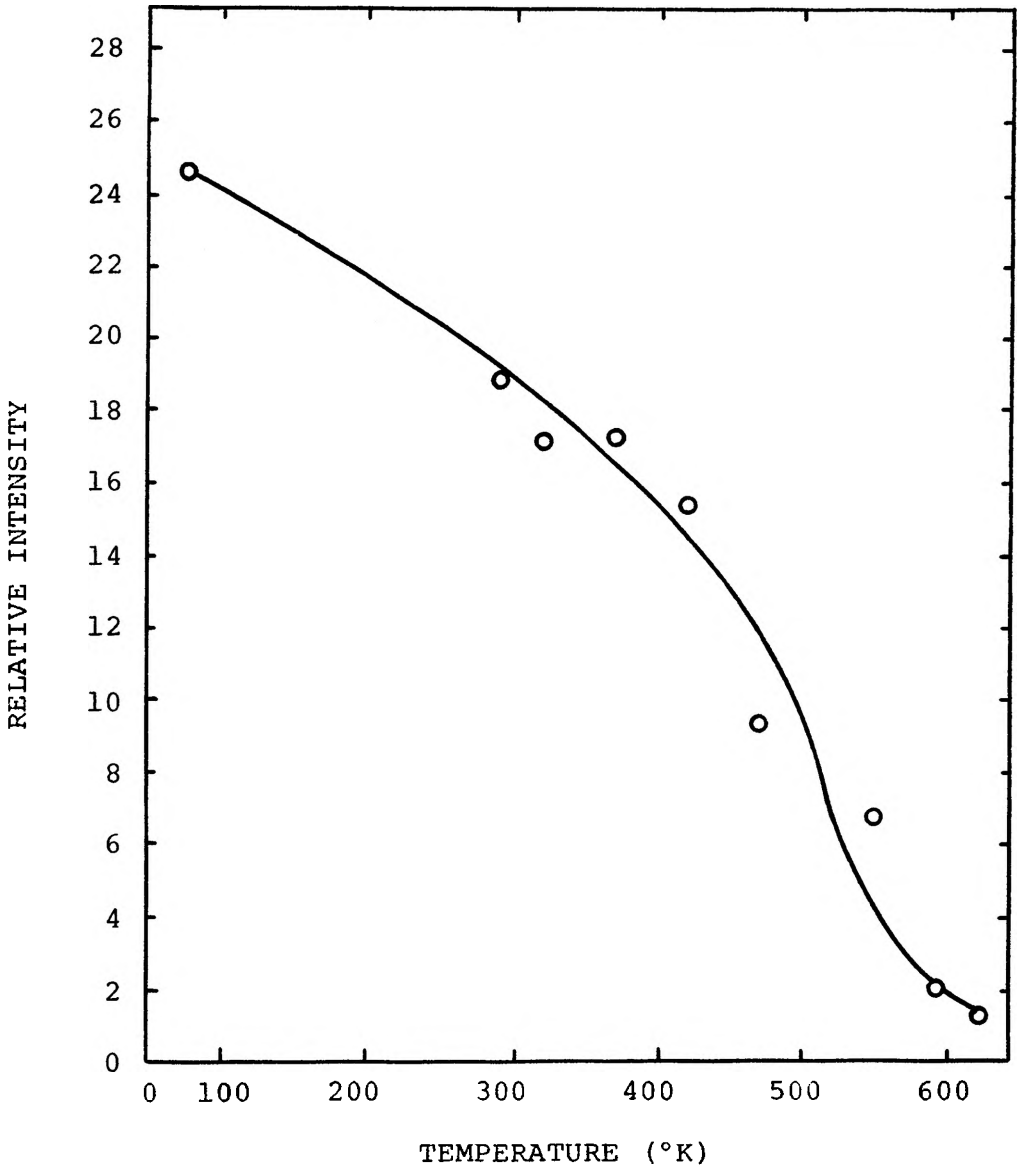

Figure 16. Temperature dependence of $HoFe_3$ (003) peak intensity.

that the easy direction of magnetization lies along the a-axis.

C. Intensity Vs. Temperature Study of $HoFe_3$

Schweizer[14] observed that the intensity of (00ℓ) magnetic peaks in neutron diffraction patterns of $HoCo_3$ fell off drastically at room temperature compared to those at 4.2°K. This implies that the easy direction of magnetization changed from the basal plane to parallel to the c-axis within this temperature range. To determine whether the same change would occur in $HoFe_3$, high temperature neutron diffraction scans were carried out on the (003) peak at various temperature intervals from room temperature to 623°K. As shown in Fig. 16 a gradual decrease in intensity occurs with increasing temperature with no discontinuities. Accordingly, in contrast to $HoCo_3$, the easy direction of magnetization of $HoFe_3$ remains in the basal plane.

V. CONCLUSIONS

High and low temperature neutron diffraction measurements were made on $HoFe_3$ and Ho_2Fe_{17} to determine their magnetic structure. Both compounds are found to have a simple ferrimagnetic structure, as found previously also in $HoFe_2$[12] and Ho_6Fe_{23}[11], with the holmium moments antiparallel to the iron moments. This type of magnetic structure is analogous to that found in the corresponding compounds containing cobalt and nickel.

An average saturation moment of $9.72\mu_B$ for holmium in Ho_2Fe_{17} at 77°K indicates that little, if any, crystal field splitting of the holmium moments occurs, as this value is nearly equal to the calculated value of $10\mu_B$ for the trivalent ion. The moment of holmium in $HoFe_3$ is not completely saturated at liquid nitrogen temperature with an average value of $8.88\mu_B$. The corresponding saturation moment should approximate that of the free trivalent ion based upon the magnetization curve of Hoffer and Salmans[13], the behavior of other RFe_3 compounds, and the remaining holmium-iron compounds. The moment of holmium behaves similarly in $HoFe_2$ and Ho_6Fe_{23} with average saturation values of 9.5 and 9.3 μ_B respectively.

The mean values for the iron saturation moments in these holmium-iron compounds are $1.7\mu_B$ in $HoFe_2$, $2.25\mu_B$ in Ho_6Fe_{23} and $2.1\mu_B$ in Ho_2Fe_{17}. The value observed at 77°K, though not at saturation, in $HoFe_3$ is $1.64\mu_B$. The fact

that the iron moment is relatively independent of the amount of rare earth present should be noted. A similar behavior is found in the dysprosium-iron[24], erbium-iron[25], yttrium-iron[26], lutecium-iron[26], and gadolinium-iron[26] systems. The average iron moment for all compounds in the Dy-Fe system is $2.1\pm0.1\ \mu_B$ and $2.0\pm0.1\ \mu_B$ in the Er-Fe system. This behavior is quite different from that found in isostructural compounds with cobalt and nickel where the transition metal moment is found to depend on the rare earth concentration within the alloy. For example, no moment is detected for Co in YCo_2[27].

For the cobalt and nickel compounds the decreasing moment with increasing rare earth concentration is explained as a filling of the 3d band of cobalt and nickel by the conduction electrons of the rare earth whereas in the iron compounds conduction electron transfer seems to play a secondary role. The primary factor in this case is the iron-iron interatomic distances and the number of iron nearest neighbors as illustrated by precise lattice parameter studies of many R_2Fe_{17} compounds by Givord et al.[6].

X-ray powder pattern studies using a pseudo-rotating-crystal method were carried out at room temperature on field-oriented $HoFe_2$, $HoFe_3$, and Ho_2Fe_{17} to determine their easy direction of magnetization. It was found to lie along a {100} direction in $HoFe_2$. The easy direction of magnetization lies in the basal plane along the b-direction in $HoFe_3$ and along the a-axis in Ho_2Fe_{17}. It is interesing

to note that these directions are physically the same. The basal plane of the primative cell of Ho_2Fe_{17} contains three basal planes of the primative cell of $HoFe_3$. When the easy direction of magnetization for each compound is plotted on such a combined coordinate system it is seen (Fig. 17) that both lie in the same direction.

Intensity versus temperature studies of the (003) peak of $HoFe_3$ indicate that the easy direction of magnetization does not move out of the basal plane, as contrasted to $HoCo_3$. The anisotropy forces of the iron sublattice are thus weaker than those of cobalt in accord with the fact that cobalt exhibits a higher coercive field than that of iron.

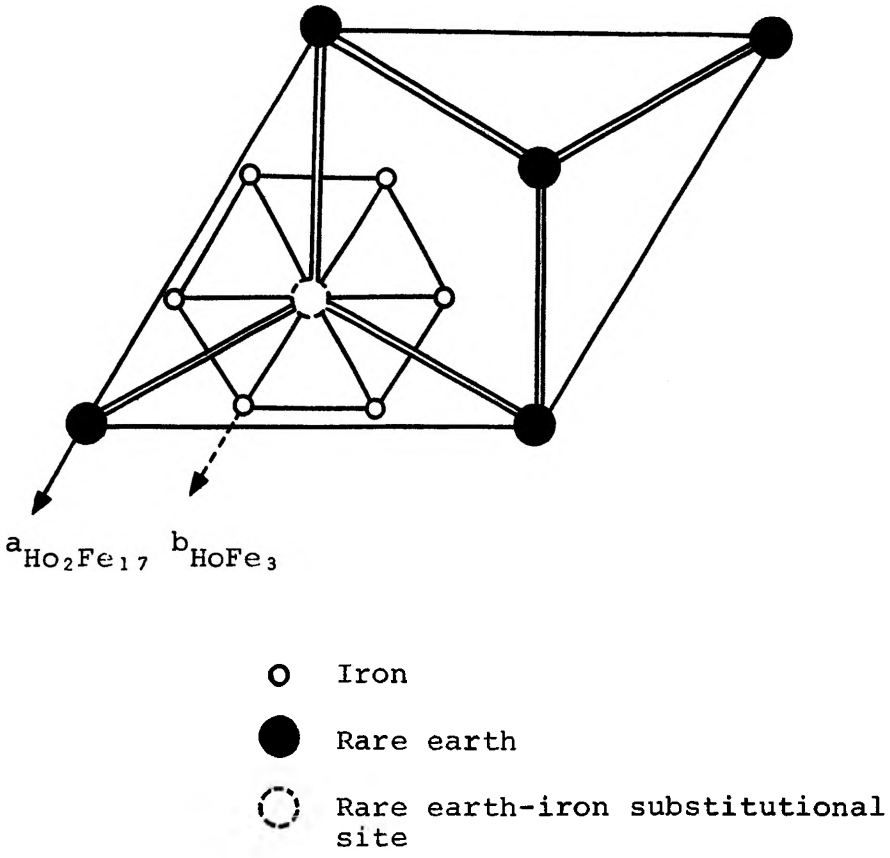

Figure 17. Easy direction of magnetization of Ho_2Fe_{17} (a) and $HoFe_3$ (b).

VI. FUTURE STUDIES

In furthering the search for both improved permanent magnet materials and knowledge of the dependence of magnetic properties upon composition, some exploratory work has been done in designing ternary alloys. Since the family of rare earth-cobalt compounds described by the formula RCo_5 exhibits extremely large magnetocrystalline anisotropy and relatively large saturation magnetization, efforts have been directed solely towards making alloys which form in the $CaCu_5$ structure. In addition, samarium-cobalt magnets cost about $40 per pound, making it highly desirable to develop materials of nearly equal magnetic properties at lower cost.

Recent work by Tsugio Shibata et al.[28] shows the coercive forces and induced magnetic anisotropies of $Y_{1-x}Sm_xCo_5$ alloys to vary in a manner similar to that of the "a" lattice parameter. The magnetic behavior thus appears to be quite dependent upon cell dimensions. Lattice parameters of $SmCo_5$, i.e., a=5.004 A° and c=3.969 A°[24], have been assumed to be optimum and attempts have been made to make new alloys with approximately the same unit cell size.

The first alloy to be made was $Y_{0.92}Ca_{0.08}Co_5$. Calcium was added to YCo_5, a=4.937 A° and c=3.978 A°[14], hopefully to increase the "a" parameter. This did not occur. The "a" parameter decreased to 4.84 A° while "c" increased

to 4.03 A°. There appeared to be a great deal of vapor coming from the metal pieces during melting. This was probably calcium since similar behavior was not observed when melting other yttrium-cobalt alloys. Alloy composition was undoubtedly changed as shown by the presence of lines from the Y_2Co_{17} phase in the x-ray powder pattern.

The next ternary alloys studies were $Y_xLa_{1-x}Co_{4.8}$ where x=1.0, 0.8, 0.6, 0.4, and 0.0. Lanthanum was chosen for two reasons. First, it has a relatively large radius and hopefully would increase the "a" lattice parameter. Second, lanthanum is only one-third the cost of yttrium and samarium and its addition could be instrumental in lower cost per pound of the end magnetic material. A cobalt composition of 4.8 was chosen instead of 5 to decrease the possibility of getting the Y_2Co_{17} or the $LaCo_{13}$ second phase. Single phase $CaCu_5$ structures were obtained for x=1.0, 0.8, and 0.6. The difficulty in obtaining single phase material for $x \leq 0.4$ is believed to be due to the much larger (liquid + solid) region above the peritectically formed $LaCo_5$ as compared to that above YCo_5, thus requiring a very rapid cooling rate to prevent the formation of the second phase. The dependence of lattice parameters upon lanthanum content is shown in Fig. 18 for the single phase alloys. The values for YCo_5[15], $LaCo_5$[29], and $SmCo_5$[30] were obtained from the literature. Although only two intermediate alloys have been made, it appears that a value of x=0.58 would produce a $CaCu_5$ structure with cell parameters

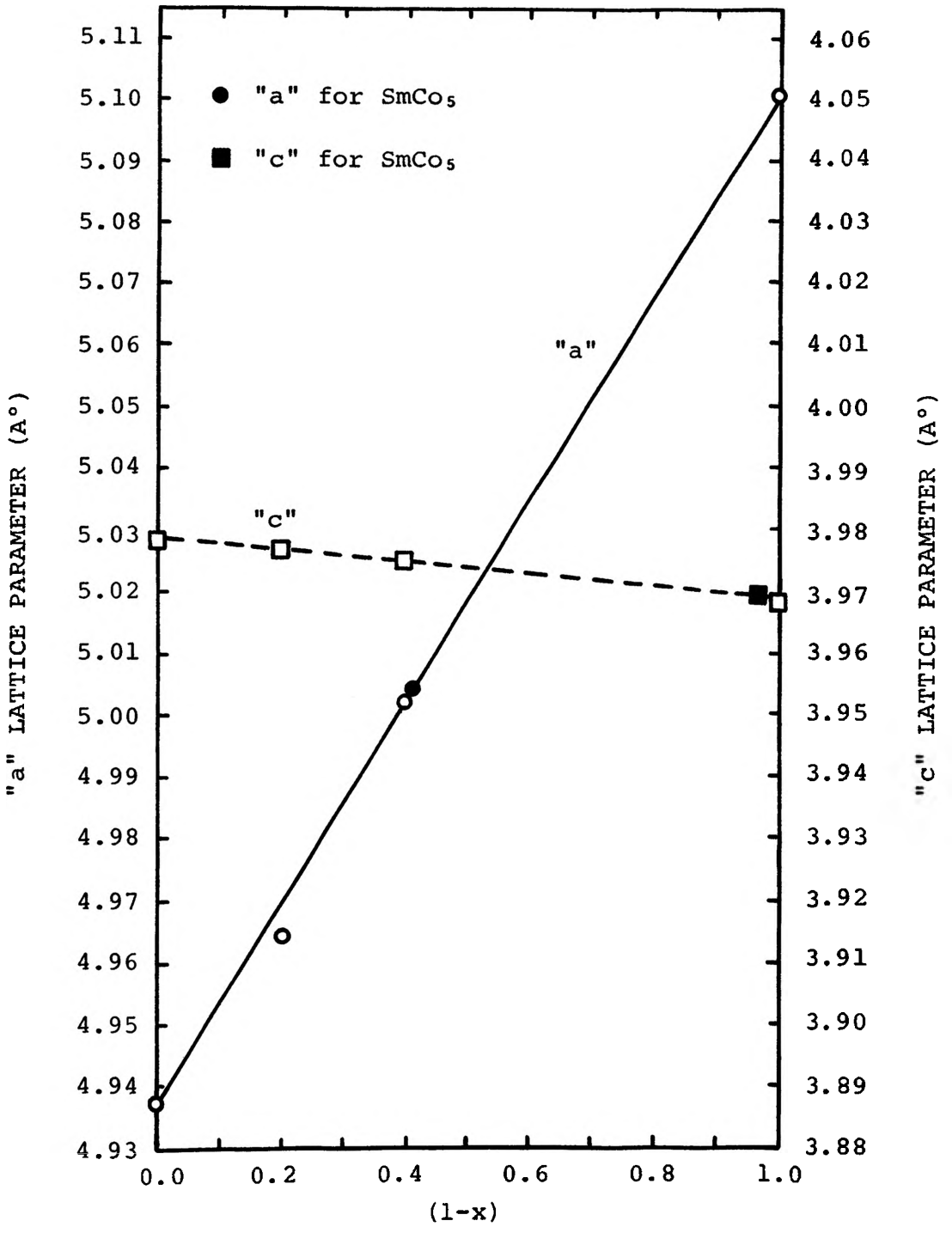

Figure 18. Lattice parameter dependence upon composition for $Y_xLa_{1-x}Co_{4.8}$ alloys.

very nearly equal to those of $SmCo_5$. This alloy and additional alloys should be made to establish the compositional boundaries within which the $CaCu_5$ structure is stable. Lattice parameter measurements and magnetic properties of these alloys must also be completed to broaden the understanding of the relationship of the magnetic behavior to composition and structure.

Following the above work should come lattice parameter, magnetization, and coercive force measurements of the quaternary alloy series $Y_xLa_{1-x}Co_yFe_{4.8-y}$. An interesting point in considering such alloys is the fact that the iron atoms might possibly order in this structure. This is certainly possible since there are two nonequivalent crystallographic sites for the transition metal atoms to occupy and the iron moments in the rare earth-iron compounds have been found to be highly localized. Essential for the determination of transition atom positions within such ordered structures is neutron diffraction. X-ray diffraction methods would be of little value due to the nearly identical scattering factors for iron and cobalt. However, in the case of neutron radiation, the nuclear scattering length of iron is nearly four times that of cobalt, being 0.96 and 0.25×10^{-12} cm.[21] respectively.

If successful, an alloy in this series will be less expensive to manufacture than $SmCo_5$ and combine the high remanent magnetization of iron with the high coercive

force of cobalt. Magnetic structure determinations by means of neutron diffraction of a few well chosen alloys in this group should be of considerable value in understanding substitutional and magnetic behavior of iron and cobalt, in combination, in permanent magnet materials.

REFERENCES

1. Roe, G. J. and O'Keefe, T. J., Met. Trans., 1, 2565 (1970).

2. Wernick, J. H. and Geller, S., Trans. Met. Soc. AIME, 218, 867 (1960).

3. Crouver, D. and Olsen, C. E., Act. Cryst., 12, 689 (1959).

4. Kripyakevich, P. I. and Frankevich, D. P., Soviet Phys. Cryst., 10, 468 (1966).

5. Florio, J. H., Baenzinger, N. C. and Rundle, R. E., Act. Cryst., 9, 371 (1956).

6. Givord, D., Lemaire, R., James, W. J., Moreau, J. M. and Shah, J. S., Proc. IEEE, to be published.

7. O'Keefe, T. J., Roe, G. J. and James, W. J., J. Less-Common Metals, 15, 357 (1968).

8. Lemaire, R. and Paccard, D., Bull. Soc. Fr. Min. Crist., 92, 9 (1969).

9. Wernick, J. H. and Geller, S., Act. Cryst., 12, 662 (1959).

10. Lonsdale, K., International Tables for X-Ray Crystallography, Vol. I (Birmingham, England: Knyoch Press, 1969) 273.

11. Roe, G. J., O'Keefe, T. J., Moreau, J. M., Michel, C. and James, W. J., Colloques Internationaux du C.N.R.S., Grenoble, mai, 2, 251 (1969).

12. Moreau, J. M., Michel, C., Simmons, M. F., O'Keefe, T. J. and James, W. J., Proc. Eighth Rare Earth Research Conf., 1, 34 (1970).

13. Hoffer, G. I. and Salmans, L. R., unpublished, presented at Seventh Rare Earth Research Conf. (1968).

14. Schweizer, J., D. Sc. Thesis, Un. of Grenoble, Sept. (1968).

15. Lemaire, R., Cobalt, 32, 137 (1966).

16. Roe, G. J., Ph.D. Thesis, Un. of Missouri-Rolla, (1969).

17. Bunn, C. W., Chemical Crystallography, (Oxford: Clarendon Press, 1963) 147.

18. Stout, G. H. and Jensen, L. H., X-ray Structure Determination, (London, England: The Macmillan Company, 1970) 83.

19. Becker, J. J., Luborsky, F. E. and Martin, D. L., IEEE Trans. Magnetics, MAG-4, 84 (1968).

20. Moreau, J. M., Michel, C., Simmons, M. F., O'Keefe, T. J. and James, W. J., J. De Physique, 32, Suppl. 2-3, C1-670 (1971).

21. Bacon, G. E., Neutron Diffraction, (Oxford: Clarendon Press, 1967) 31.

22. Shirane, G., Act. Cryst., 12, 282 (1959).

23. Bowden, G. J., Proc. Phys. Soc., 1, 1376 (1968).

24. Van Der Goot, A. S. and Buschow, K. H. J., J. Less-Common Metals, 21, 151 (1970).

25. Buschow, K. H. J. and Van Der Goot, A. S., Phys. Stat. Sol., 35, 515 (1969).

26. Givord, D., Givord, F. and Lemaire, R., J. De Physique, to be published.

27. Lemaire, R., Cobalt, 33, 201 (1966).

28. Shibata, T., Katayama, T. and Mizuhara, T., Japan J. Appl. Phys., 10, 163 (1971).

29. Buschow, K. H. J. and Velge, J. J., J. Less-Common Metals, 13, 11 (1967).

30. Velge, J. J. and Buschow, K. H. J., J. Appl. Phys., 39, 1717 (1968).

VITA

Michael Fred Simmons was born on January 15, 1942, in Quincy, Illinois. He received his high school education from Quincy Senior High School, Quincy, Illinois. After graduating from high school, he attended the University of Missouri-Rolla, Rolla, Missouri. He received a Bachelor of Science degree in Metallurgical Engineering in May 1964.

In June 1964, he entered graduate school at Iowa State University, Ames, Iowa and was awarded a Master of Science degree in Metallurgy in November 1966. He remained in graduate school at Iowa State University through April 1967, completing most of the course requirements for a Ph.D. degree.

In July 1967 he entered military service as a First-lieutenant in the Ordnance Corps, U.S. Army and after completing his initial orientation at Aberdeen, Maryland spent the remainder of his tour assigned to the Office of Data Systems, Ft. Lee, Virginia. He spent his second year of active duty in the rank of Captain.

He has been enrolled in the Graduate School of the University of Missouri-Rolla since July 1969 and has held a Space Science Research Assistantship at the Graduate Center for Materials Research for the period July 1969 through December 1971.

On September 1, 1963 he married the former Donna Kay Ehrhardt of Quincy, Illinois. He has two children, Nicole born June 1, 1968 and Nathan born July 29, 1970.

APPENDIX A

DISCUSSION OF MAGNETIC SCATTERING VECTORS

The magnetic interaction vector, $\vec{q}$, is defined in terms of two unit vectors $\vec{\varepsilon}$, and $\vec{K}$, by the following equation

$$\vec{q} = \vec{\varepsilon}(\vec{\varepsilon}\cdot\vec{K}) - \vec{K}.$$

The scattering vector, $\vec{\varepsilon}$, is normal to the reflecting plane while $\vec{K}$ is parallel to the magnetic moment of the scattering atom. By denoting the angle between $\vec{\varepsilon}$ and $\vec{K}$ as α, we find

$$q^2 = \vec{q}\cdot\vec{q} = [\vec{\varepsilon}(\vec{\varepsilon}\cdot\vec{K}) - \vec{K}]\cdot[\vec{\varepsilon}(\vec{\varepsilon}\cdot\vec{K}) - \vec{K}]$$

$$\text{but } \vec{\varepsilon}\cdot\vec{K} = |\vec{\varepsilon}||\vec{K}|\text{Cos }\alpha = \text{Cos }\alpha$$

$$q^2 = [\vec{\varepsilon}(\text{Cos}\alpha) - \vec{K}]\cdot[\vec{\varepsilon}(\text{Cos}\alpha) - \vec{K}]$$

$$= \vec{\varepsilon}(\text{Cos}\alpha)\cdot\vec{\varepsilon}(\text{Cos}\alpha) - 2[\vec{\varepsilon}(\text{Cos}\alpha)\cdot\vec{K}] + \vec{K}\cdot\vec{K}$$

$$= \text{Cos}^2\alpha - 2\text{Cos}^2\alpha + 1$$

$$= 1 - \text{Cos}^2\alpha$$

$$= \text{Sin}^2\alpha$$

Fig. 19(a) illustrates general orientations of these vectors in relation to a crystallographic plane. Figs. 19(b) and (c) show two limiting cases for $\vec{\varepsilon}$ and $\vec{K}$ arrangements. In (b), where the scattering vector is parallel to the atom magnetic moment, $\alpha=0$ and $q^2=0$, i.e., there will be no magnetic contribution to the intensity from this atom and only the nuclear intensity will be seen However, when $\vec{\varepsilon}$ is perpendicular to $\vec{K}$, i.e., $\vec{K}$ lies within the reflecting plane, as in (c), $\alpha=90°$ and $q^2=1$. In this case

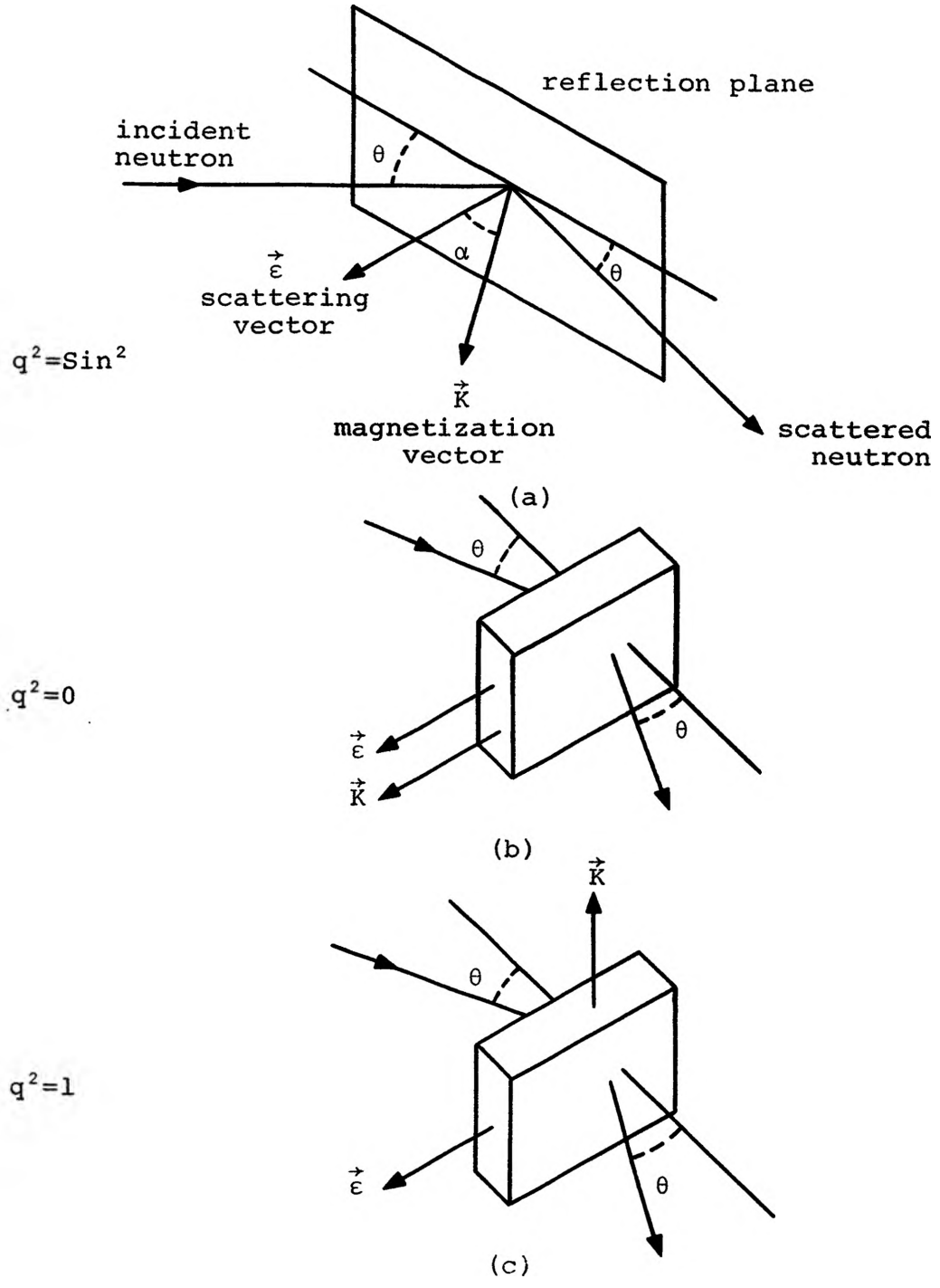

Figure 19. Identification of the unit vectors used in the discussion of magnetic scattering.

the intensity will be equal to the sum of $F_n^2 + F_m^2$.

In reality, q^2 can have values between these two limits and is found in the case of random magnetic moment orientations to have a value of 2/3. Although F_m may have the same value for several equivalent planes, due to multiplicity, a different q^2 value may be associated with each plane. An average value $\langle q^2 \rangle$ is therefore usually used which is then multiplied by the multiplicity factor.

Reference is again made to the article by Shirane[22] if a more detailed explanation is desired.

APPENDIX B

MAGNETIC FORM FACTORS

The following plots of experimentally determined magnetic form factors for holmium and iron were obtained from D. W. C. Koehler, Oak Ridge National Laborabory, Oak Ridge, Tennessee.

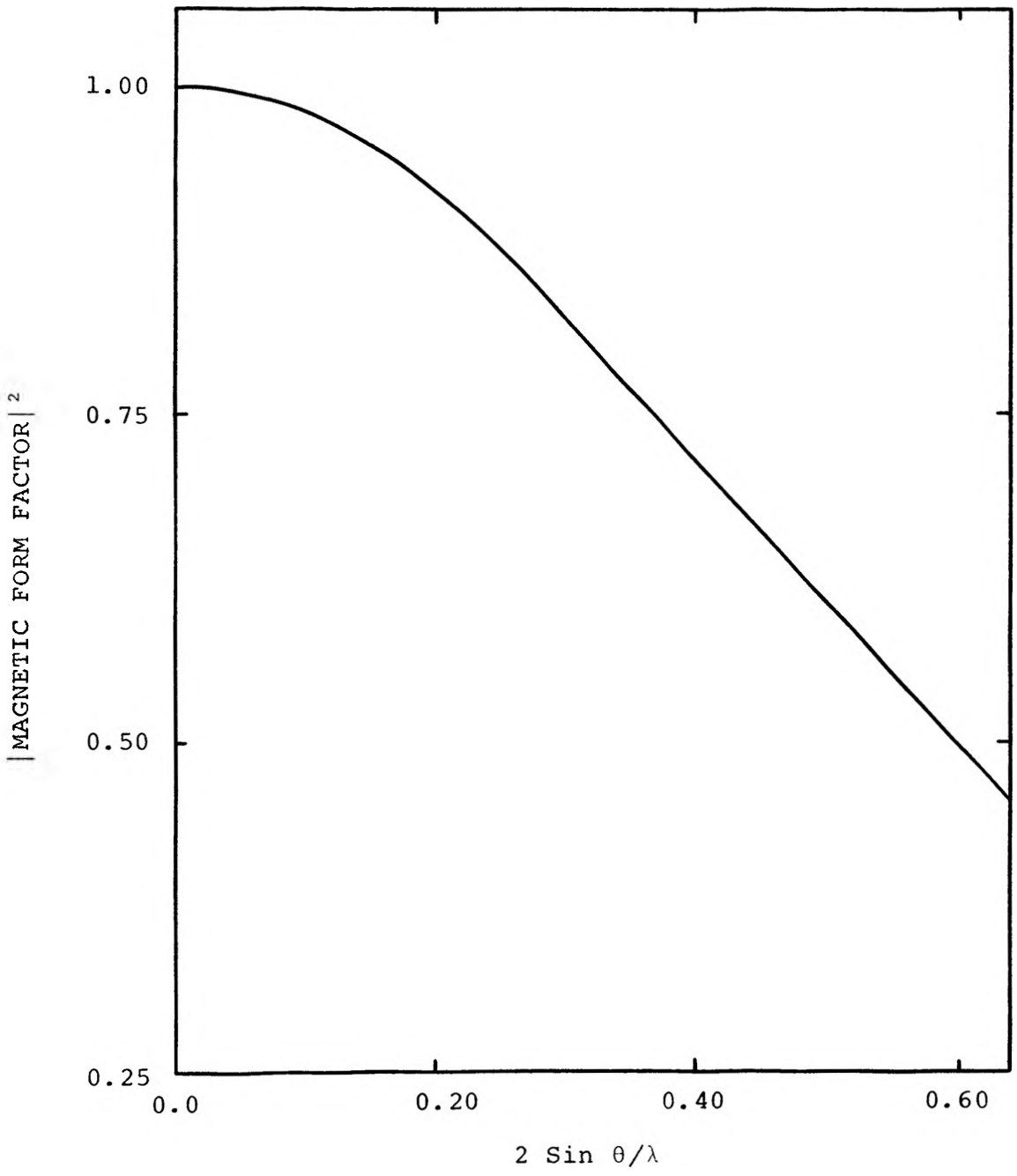

Figure 20. Magnetic form factor for holmium.

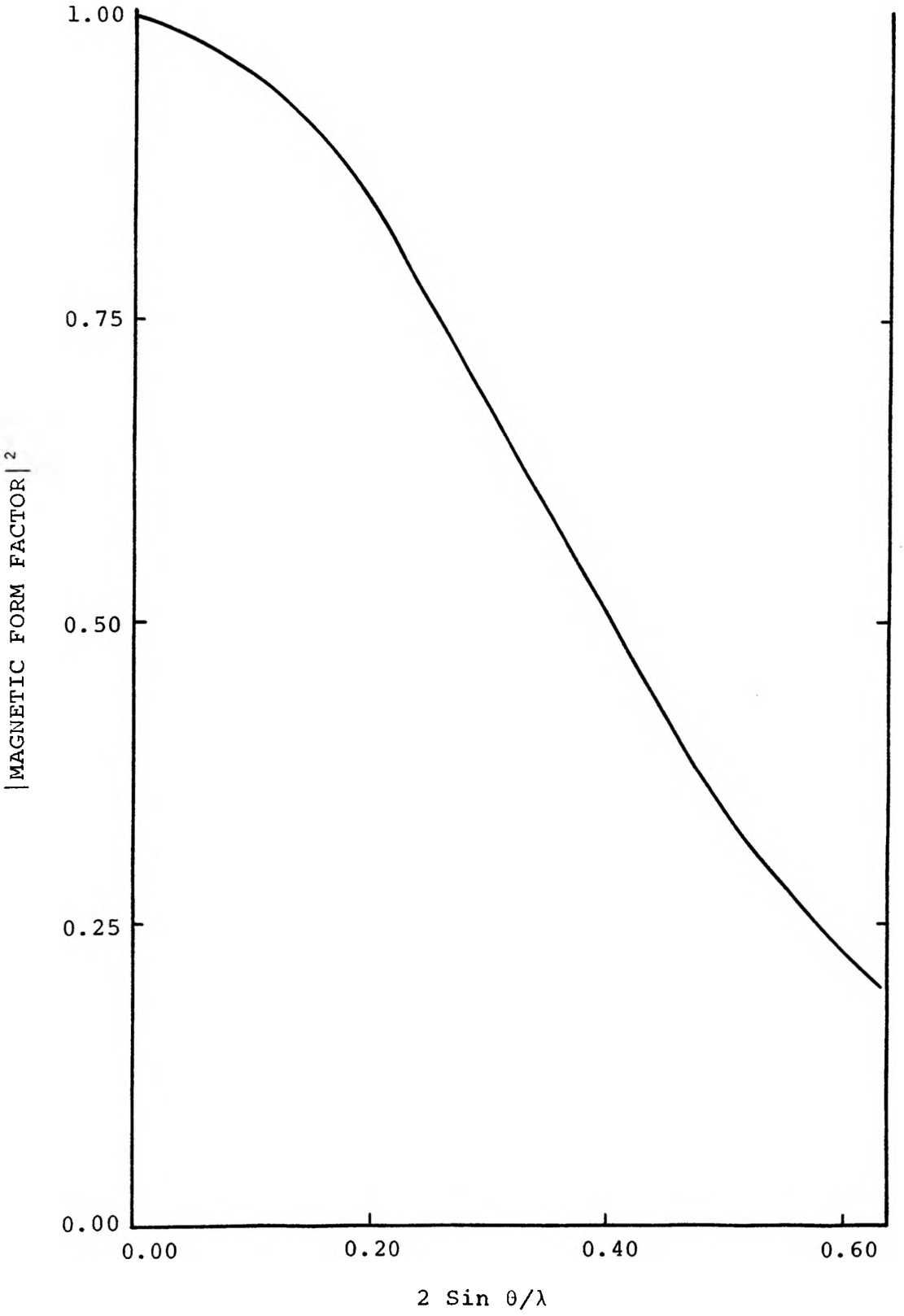

Figure 21. Magnetic form factor for iron.

APPENDIX C

METALLOGRAPHY

Although difficulties were initially encountered during metallographic preparation because of extreme pitting both during polishing and etching, satisfactory results were obtained using the following procedure.

1. Mount specimen using commercial cold-mounting material to avoid heating the sample.

2. Rough grind to obtain a flat surface using a belt sander with frequent cooling of the mounted specimen by dipping in water.

3. Dry polish on emery paper through 600 grit taking care to thoroughly rinse any particles from the specimen surface with methyl alcohol when changing grit size.

4. Polish on nylon-cloth covered wheel using #9 diamond polishing compound and oil.

5. Polish on a different nylon-cloth covered wheel using #1 diamond polishing compound and oil.

6. Final polish on a microcloth using a slurry of 0.05 micron alumina powder and distilled water.

7. Etch with 4% nital.

8. Thoroughly clean sample ultrasonicly in a methanol bath between each wheel polishing above.